Full length article

Theory of double-kink nucleation in dilute BCC alloys

Alireza Ghafarollahi*, William A. Curtin

Laboratory for Multiscale Mechanics Modeling (LAMMM), Institute of Mechanical Engineering, EPFL Lausanne 1015, Switzerland

ARTICLE INFO

ABSTRACT

Yielding in pure BCC metals and dilute substitutional alloys occurs by double-kink nucleation and propagation along screw dislocations. At low temperatures, the yield stress is controlled by double-kink nucleation. Here, an analytical statistical model is presented to predict the stress- and length-dependent double-kink nucleation barrier in dilute BCC alloys solely in terms of the double-kink process in the pure metal and the solute/screw-dislocation interaction energies in the dilute alloy. Consistent with early literature, dilute alloying always reduces the double-kink nucleation barrier (softening) independent of solutes or matrix. The model is extensively validated via simulations in model Fe-Si alloys described by interatomic potentials. The model is then compared to experiments on real Fe-Si, W-Ta, and W-Re alloys, showing qualitative agreement consistent with the accuracy of the inputs. A cross-over from the dilute limit to the non-dilute limit, where there is hardening, is analyzed using the present theory and the non-dilute theory of Maresca et al. The analysis for Fe-Si is consistent with a cross-over at $\approx 2-3$ at.%Si, as observed experimentally, and qualitatively consistent with W-Ta and W-Re. The present theory plus the recent theory of Maresca et al. together provide a coherent predictive framework for strengthening of screw dislocations over the full range of concentrations from extremely dilute ($\ll$ 1 at.%), to dilute (up to a few at.%) and non-dilute alloys including High Entropy Alloys.

© 2020 Acta Materialia Inc. Published by Elsevier Ltd. All rights reserved.

1. Introduction

In BCC metals and dilute substitutional alloys, plastic deformation is controlled by the thermally-activated motion of screw dislocations by a two-step process. The first step is the nucleation of a pair of kinks along an initial long straight screw dislocation. The second step is the migration of these kinks along the screw that ultimately advances the entire screw dislocation forward by one Peierls valley. In pure BCC metals, the double-kink nucleation is the rate-limiting process because kink migration has a negligible barrier. In dilute solid solution BCC alloys, the solutes modify the barriers for both double-kink nucleation and kink migration. The controlling process is that with the largest barrier; this requires a statistical determination of the relevant barriers as a function of the applied stress and concentration. In general, the double-kink nucleation barrier is reduced by solutes because nucleation occurs in that region where the solute fluctuations in the random alloy will most-favor formation of the double kink. Kink migration must then overcome the largest solute-induced barriers for migration along the remaining line length. With increasing solute concentration, the conventional understanding is that the nucleation

barrier is steadily reduced and the kink migration barrier steadily increased such that there can be a cross-over from control by nucleation to control by migration. This can lead to a transition from softening (reduced flow stress, relative to the pure metal, with increasing concentration) to hardening (increasing flow stress with increasing concentration). Such behavior has been predicted via models [1] and observed in recent Monte Carlo simulations in both Fe-Si [2] and W-Re [3], although results depend on details of the models and simulation methods.

The softening by solutes in the dilute limit was recognized long ago [4–6]. Considering the attractive force of impurity atoms on a dislocation line, Weertman [4] showed that the impurity atoms could reduce the Peierls energy in their immediate neighborhood, leading to a reduction in the required stress. Softening can be achieved, however, with either attractive or repulsive solutes (see Fig. 1). For repulsive solutes, an initial straight dislocation is simply pushed away from the solute, and the double-kink nucleation barrier is reduced. There is substantial evidence of softening due to small additions of many solutes in many BCC elements at low temperatures [5,7]. Suzuki [6] developed a statistical model for solute effects on double-kink nucleation and kink-migration processes. He envisioned a single solute/dislocation interaction energy E_0 and considered that somewhere along the dislocation line there could be m solutes within the double-kink nucleation length. Suzuki then postulated that the decrease in double-kink nucleation
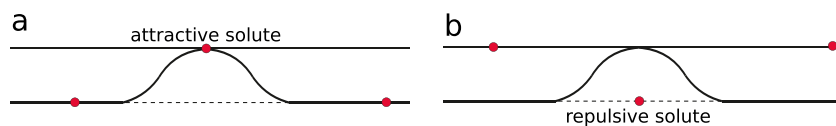
Fig. 1. (a) An attractive and (b) a repulsive solute pulling and pushing the initial dislocation line away, respectively, towards the next Peierls valley. In both cases, the double-kink nucleation barrier is reduced.

energy would be $-m|E_0|/2$ where the absolute value accounts for the fact that both attractive and repulsive solutes could reduce the barrier and where the factor of 1/2 was postulated as the reduction in barrier following simple chemical kinetics models. The value of m was then computed as the largest value along a dislocation line length L. The Suzuki model thus contains the key features of the problem, but with crucial assumptions about the solute/dislocation interaction energies and their effects on the nucleation barrier that limit quantitative predictions. That is, the single parameter E_0, the statistical factor m, and the factor of 1/2, are all ad-hoc approximations that are not accurate in realistic systems.

In spite of the above early studies, the recent literature [1,8] makes a different set of assumptions. Retaining only a single solute/dislocation interaction energy E_0, these works postulate that the rate of double-kink nucleation along a long line is changed by the factor $c\,e^{-E_0/kT}$ where c is the solute concentration. This model thus effectively considers only individual solutes (the very dilute limit) with no statistical effects and, moreover, predicts that repulsive solutes ($E_0 > 0$) decrease the double-kink nucleation rate (leading to increased yield stress). Solutes with positive and negative interaction energy are thus predicted to be fundamentally different[8] (hardening vs. softening). This is in conflict with experiments at the yield point. For instance, as shown later below, data of Stephens [7] shows softening at low temperature and low solute concentrations for both W-Ta and W-Re alloys even though first-principles DFT predicts the interaction energy of Ta to be positive and that of Re to be negative [8] (see Fig. 2(a) and (c)). Other comparisons with experiments were made using hardness data [1], corresponding to plastic strains of ~ 7-10% while the data in Ref. [7] shows that behavior at yield and at a few percent plastic strain can lead to conflicting conclusions regarding softening versus hardening.

Prior analyses [1,9] also included an additional direct change to the Peierls stress in an alloy. This contribution can be viewed as the Peierls stress of the effective homogeneous representation of the alloy. Such a representation is important at non-dilute concentrations where the identities of solute and matrix become less clear [10]. In the dilute limit, the explicit dominant effects of the individual solute additions are clear and provide perturbations to the double-kink nucleation barrier of the underlying matrix material. These effects change the apparent Peierls stress, as discussed below, with no additional considerations.

Here, in light of the limitations of previous analyses as sketched above, we re-consider double-kink nucleation in the presence of low concentrations (a few percent or below) of solutes. We present and validate a general analytical statistical model for the effects of solutes on the double-kink nucleation barrier as a function of concentration and applied stress. This model is a significant improvement over the simplified model of Suzuki, and reveals the limitations of other models. It should be noted that all screw-dislocation-based theories to date including the present model assume that the screw dislocation core is the well-defined compact symmetric core. This is true for dilute alloys [8,11–13] of interest here, but first-principles studies by Rao et al. [14], Romaner et al. [10], and Li et al. [15] show that screw cores may not always remain symmetric and compact in some non-dilute alloys.

In applications of the model, we obtain reasonable agreement with experiments at low concentrations where double-kink

nucleation is expected to dominate. With increasing concentration, we then show a cross-over from softening, controlled by the present theory, to hardening, controlled by the recent non-dilute theory of Maresca and Curtin [16]. The Maresca-Curtin theory argues that the low-energy state of a screw dislocation is intrinsically kinked over a characteristic length scale, making double-kink nucleation irrelevant. The cross-over from softening to hardening is then mainly related to whether the spacing of the intrinsic kinks is smaller than the typical dislocation length between dislocation junctions. If not, then the dilute theory (softening) applies. If so, then the non-dilute theory (hardening) applies. The strength in the non-dilute domain of the Maresca-Curtin theory is still controlled by some combination of kink-migration, cross-kink formation/pinning of screws, and, at very low temperatures, a Peierls-like motion. These features are similar to, although different in detail than, those postulated by Suzuki [6]. So, both new [16] and old [6] theories, while different, show that double-kink nucleation does not control strengthening at higher concentrations. The present theory and that of Maresca et al. thus bridge across the full composition range of BCC alloys from very dilute up to multicomponent non-dilute High Entropy Alloys.

The remainder of this paper is organized as follows. In Section 2, we discuss the effect of multiple solutes on the double-kink nucleation barrier. A statistical model to predict the double-kink nucleation barrier as a function of solute concentration, dislocation length, and applied stress is presented. The effect of single solutes, relevant in the very dilute limit, is addressed in Section 3. In Section 4, we validate our analytic statistical model using atomistic simulations on a model Fe-Si alloy. In Section 5, we discuss the general application of our results, make specific comparisons for Fe-Si, W-Ta, and W-Re, show the cross-over from dilute to non-dilute in Fe-Si, and discuss further implications of our work. Section 6 summarizes the paper.

2. Solute effects on the double-kink nucleation barrier

2.1. Basic quantities

We consider a binary dilute alloy in which there is only one type of substitutional solute at concentration c and the other component has a high concentration and serves as the "matrix". The model is easily generalized to multiple components. The solute concentration c is low (below a few percent) but above a "very dilute limit" defined later by a critical concentration c^*. We consider solutes for which the maximum interaction energy change as a dislocation moves past an individual solute is smaller than the single dislocation kink energy. Then, an individual solute does not create a kink migration barrier that is larger than the solute-reduced kink nucleation barrier. Since kink energies are estimated to be 0.45 eV or larger [18], this limit holds for many substitutional solutes in most BCC metals although there are exceptions such as Co, Rh, Ir, Ni, Pd, and Pt in W according to DFT results of Hu et al. [8]. Interstitial solutes may also have large interaction energies, and so are not considered here.

Underpinning double-kink nucleation in the alloy is the stress-dependent double-kink nucleation barrier and transition state in the pure matrix. Fig. 3 shows the transition state configurations for pure Fe at various applied stresses, as obtained using a reasonable
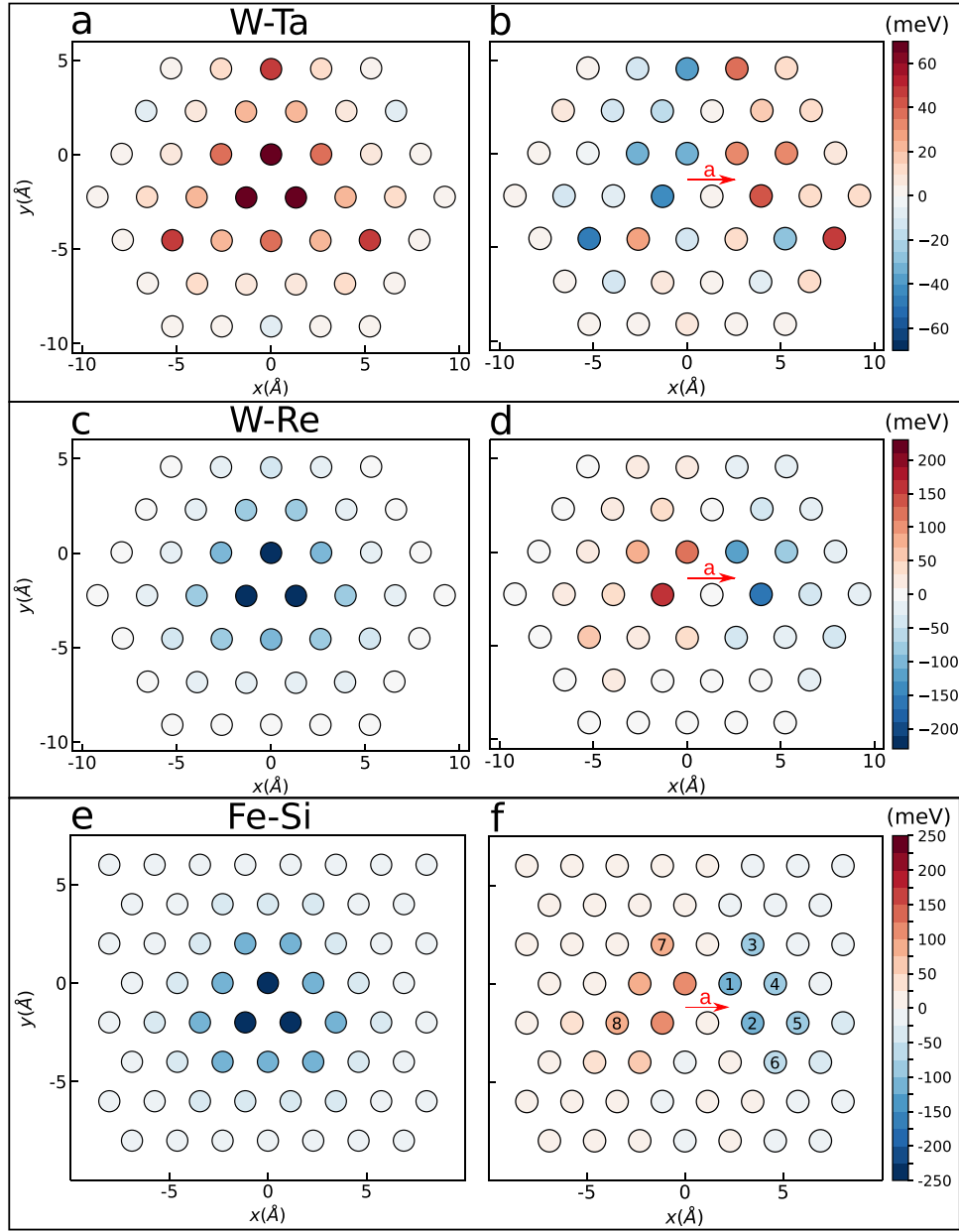
Fig. 2. Solute/screw dislocation interaction energy versus solute position for **a** Ta [8,17] and **c** Re [8,17] in single crystal BCC W as calculated by DFT and **e** Si in Fe as computed using the EAM potential of [2]. Interaction energy difference as the screw dislocation core moves by one Peierls valley distance a (red arrow) for **b** Ta and **d** Re solutes in W and **f** Si in Fe. Sites marked with 1–8 in **f** are substituted with Si atoms for subsequent NEB calculations, and are referred to in Figs. 5 and 6. (For interpretation of the references to colour in this figure legend, the reader is referred to the web version of this article.)
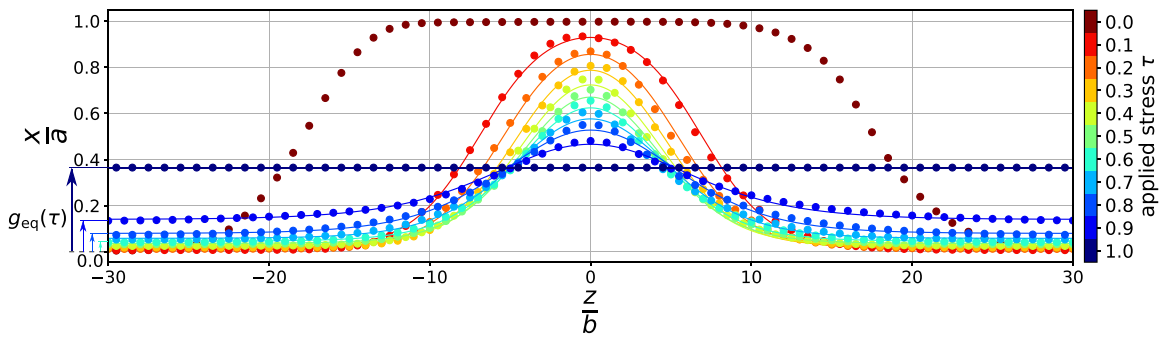

Fig. 3. Transition state configurations $x_{\text{disl}}(z, \tau)/a$ versus applied shear stress τ determined using pure Fe EAM potential [19]. The points are the direct outcome of the disregistry method [22]. The solid lines are the fits to the functional form for $g(z, \tau)$ given by Eq. (19) with parameters shown in Table 1. On the lower left, the equilibrium position $g_{\text{eq}}(\tau)$ of the initial straight dislocation is indicated by the arrows for several applied stresses.

Table 1
Parameters describing the transition state configurations for double-kink nucleation of pure Fe at various normalized applied stresses, τ/τ_p. The geometrical factor, $G(\tau/\tau_p)$ is obtained by Eq. (6) with $g(z, \tau)$ given by Eq. (19) and $N_s = 10$.

τ/τ_p	$\alpha(\tau/\tau_p)$	$\zeta(\tau/\tau_p)$	$g_{eq}(\tau/\tau_p)$	$G(\tau/\tau_p)$
0.0	4.347	6.987	0.00	3.07
0.1	4.347	6.987	0.00	3.07
0.2	4.381	5.367	0.01	2.55
0.3	4.444	4.487	0.02	2.20
0.4	4.571	3.918	0.03	1.94
0.5	4.792	3.584	0.04	1.77
0.6	5.184	3.419	0.05	1.64
0.7	5.755	3.311	0.06	1.52
0.8	6.725	3.241	0.08	1.39
0.9	7.886	2.666	0.14	1.06
1	-	0	0.365	0

EAM potential for Fe [19] (see [20] for a study using a machine-learning potential and [18] for configurations obtained using a line tension model). At zero stress, the transition state is symmetric, has two fully-developed kinks, and spans 1/2 the simulation cell size. With increasing applied stress, the initial position of the dislocation moves away from the zero-stress Peierls valley to position $x_{eq}(\tau)$. More importantly, the critical double-kink configuration becomes progressively smaller: the kinks are closer together and the kink is not fully-developed. Only at low stresses does the kink extend into the next Peierls energy minimum at distance $a = 0.943\,b$ from the original minimum. An individual kink typical spans a length $> 10b$ so that the character angle θ of the kink segment is $\theta < \tan^{-1}(0.943/10) \approx 5^o$, i.e. very close to pure screw character.

The dislocation shape $x_{disl}(z, \tau)$ of the double-kink transition state versus applied stress can be expressed generally as

$$x_{disl}(z, \tau)/a = g(z, \tau) + g_{eq}(\tau) \qquad (1)$$

where $g_{eq}(\tau) = x_{eq}(\tau)/a$ is the dimenionless initial straight screw position at stress τ and $g(z, \tau)$ is the dimensionless kink shape, or deviation from the initial straight dislocation, as a function of τ, At low stresses (e.g. 100 MPa in Fig. 3), the nucleation occurs over a length l_{dk} approximately equal to that of the two kink widths. Across a range of systems, this length is $l_{dk} \approx 20b - 25b$. The geometry of the transition-state double-kink structure versus stress serves as one main input for our analysis of solute effects on nucleation.

Associated with each stress and transition state is the nucleation enthalpy barrier $\Delta H^0(\tau)$ of the pure matrix. The functional form of $\Delta H^0(\tau)$ is not directly relevant for most of our analysis below, but is needed for predictions. This barrier can be obtained by simulations, models, or fitting. The latter often takes the form of a Kocks law [21] $\Delta H^0(\tau) = \Delta H^0(0)[1 - (\tau/\tau_p)^p]^q$ where $0 \leq p \leq 1$ and $1 \leq q \leq 2$ are fitting parameters and $\Delta H^0(0)$ and τ_p are the zero-stress enthalpy barrier and Peierls stress, respectively.

The second major quantity of importance is the interaction energy between a type-n solute at position (x_i, y_j, z_k) and a straight screw dislocation positioned in the Peierls valley minimum at the origin and aligned along the z axis. This interaction energy is denoted as U_{ij}^n. Fig. 2(e) shows U_{ij}^n for many solute positions ij around the core within the periodic length b along the line direction z for Si solutes in Fe as computed using a model Fe-Si alloy described by EAM potentials [2]. The solute/dislocation interaction energies for Ta and Re solutes in single crystal BCC W as computed by Density Functional Theory (DFT) [8,17] are shown in Fig. 2(a) and (c); quantitatively similar results are reported in other works [11]. With this projection, the interaction energy is independent of the z coordinate. For the model Fe-Si and W-Re systems all solute/dislocation interactions are negative (attractive) while the interactions for Ta in W are all positive (repulsive). The interaction

energies are not localized to the first or second neighbors around the core, as commonly assumed in theories that use these computed energies to predict strengths [1,6,8].

Dislocation motion is determined by the *changes* in solute/dislocation energy as a dislocation glides. Fig. 2(f) shows the change in energy of a Si solute in Fe upon glide of the screw dislocation by one Peierls valley distance, a. Fig. 2(b) and (d) show the corresponding DFT energy changes for Ta and Re solutes in W matrix, respectively. Non-negligible changes in energy can exist for solutes located at initial positions up to sixth neighbors from the center line of the core. As discussed extensively in Ref. [23], and important in the present work, it is necessary to consider solutes out to such distant neighbors to capture the relevant energy changes accurately. These interaction energies and changes upon glide are the fundamental quantities driving double-kink nucleation in a dilute alloy.

2.2. Solute/double-kink interaction energy

Direct computation of the solute/double-kink interaction energies for all possible solute positions around the (transition state) double-kink structure is not possible. Computation of an interaction energy requires full relaxation of the system containing the solute and dislocation but the double-kink structure is a constrained state and is not a low-energy relaxed equilibrium structure. Here, we thus make a model assumption and then validate that assumption via direct simulations in Section 4.2.

We assume that the solute/double-kink interaction energy at each stress and for a single solute at position (x_i, y_j, z_k) is

$$E_{dk}(x_i, y_j, z_k, \tau) = \frac{x_{disl}(z_k, \tau)}{a} \Delta U_{ij}(a) + U(x_i, y_j), \qquad (2)$$

where $\Delta U_{ij}(a) = U(x_i - a, y_j) - U(x_i, y_j)$ is the solute/screw dislocation energy change as the dislocation moves by one Peierls valley distance a (Fig. 2b,d,f). That is, the solute/double-kink interaction energy of a solute in plane z is equal to the full energy change upon glide by a scaled by the distance x of the kink in the same z plane. This approximation is reasonable because, as shown above, the character of the kink is very near screw. Therefore, a solute experiences a surrounding region that is very nearly a straight screw dislocation at position $x_{disl}(z_k, \tau)$. This approximation also satisfies the limiting cases where the dislocation is in the initial and final Peierls valleys, i.e. $x_{disl}(z_k, \tau) \to 0$ and $x_{disl}(z_k, \tau) \to a$.

In the presence of any specific arrangement of solutes, the change in nucleation barrier is the sum of the changes, whether positive or negative, contributed by each individual solute. In the dilute limit, we can safely neglect any effects of multi-solute interactions because the average solute-solute separation is large ($\approx b/c^{\frac{1}{3}}$); each solute thus has an effect independent of any other solutes. A specific random arrangement of solutes is represented by a set of occupation variables s_{ijk} where $s_{ijk} = 1$ if a solute is at position (x_i, y_j, z_k) and $= 0$ otherwise. Overall all sites $N \gg 1$ in the alloy, $1/N \sum_{i,j,k} s_{ijk} = c$. The double-kink nucleation barrier is then the energy difference between all solutes interacting with the transition state structure $g(z, \tau) + g_{eq}(\tau)$ and with the initial straight dislocation at $g_{eq}(\tau)$, and so involves only the non-straight portion $g(z, \tau) = x_{disl}(z_k, \tau)/a$ of the transition state shape. Using Eq. (2) for the single solute/double-kink interaction energy, the solute contribution to the nucleation barrier is computed by summing the contributions of all the solutes in the specific realization of the random alloy as

$$\Delta H^{sol}(\tau) = \sum_{i,j,k} s_{ijk}\, g(z_k, \tau)\, \Delta U_{ij}(a) \qquad (3)$$

2.3. Model for solute softening in dilute alloys

For a dislocation segment of length l_{dk}, the mean energy change over all possible fluctuations in the positions of the solutes is zero. This is shown by averaging Eq. (3) over all realizations s_{ijk}. However, the local fluctuations in the spatial arrangement of solutes give rise to a statistical distribution of energy changes of the nucleated dislocation segment. The standard deviation of this energy change is

$$\sigma_{\Delta H^{\text{sol}}} = \left[\left\langle \Delta H^{\text{sol}}(l_{dk}, x_{\text{disl}})^2 \right\rangle - \left\langle \Delta H^{\text{sol}}(l_{dk}, x_{\text{disl}}) \right\rangle^2 \right]^{\frac{1}{2}}, \tag{4}$$

where brackets denote averaging over the random occupation variables s_{ijk}. Carrying out the averaging and algebra leads to (Appendix A)

$$\sigma_{\Delta H^{\text{sol}}} = \Delta \tilde{E}_p(a) \, G(\tau), \tag{5}$$

where

$$G(\tau) = \left(\sum_{k=-N_s}^{N_s} g(kb, \tau)^2 \right)^{\frac{1}{2}}, \tag{6}$$

is a geometrical shape factor and $N_s = l_{dk}/(2b)$ is the total number of atomic sites along the dislocation line z within one kink length $l_{dk}/2$. The standard deviation of the statistical distribution of nucleation barriers at length l_{dk} thus scales with the quantity

$$\Delta \tilde{E}_p(a) = \left(\sum_{ij} c \, \Delta U_{ij}(a)^2 \right)^{\frac{1}{2}}; \tag{7}$$

this is precisely the solute/screw dislocation interaction energy parameter that enters in the theory for yield strength of a BCC alloy [16,23], but reduced to the dilute binary alloy limit. This feature will later enable a bridging between dilute and non-dilute alloys. The shape of the double-kink transition state enters only as an overall stress-dependent numerical factor $G(\tau)$.

Considering one nucleation length l_{dk}, the random fluctuations in solutes leads to a Gaussian probability distribution of the solute contributions to the double-kink nucleation enthalpy ΔH^{sol} as

$$P[\Delta H^{\text{sol}}] = \frac{1}{\sqrt{2\pi}\sigma_{\Delta H^{\text{sol}}}} \exp\left[-\frac{1}{2}\left(\frac{\Delta H^{\text{sol}}}{\sigma_{\Delta H^{\text{sol}}}} \right)^2 \right]. \tag{8}$$

The above result is for a dislocation of length l_{dk} only. A longer dislocation line of length L can be considered approximately as a set of $N = L/l_{dk}$ statistically-independent segments of length l_{dk}, and double-kink nucleation could initiate at any one of these segments. Each segment has a distinct local solute configuration and hence has a local double-kink nucleation barrier that is sampled randomly from the above statistical distribution. The total rate of double-kink nucleation due to nucleation at all sites is the sum of the rates of all N segments, which can be written as (see Appendix B)

$$R = \nu_0 N \exp\left(-\frac{\Delta H^0(\tau)}{kT} \right) \exp\left(\frac{\sigma_{\Delta H^{\text{sol}}}(c, \tau)}{\sqrt{2}\,kT} \right)^2$$
$$\times \frac{1}{2} \operatorname{erfc}\left(\frac{\Delta \overline{H}^{\text{sol}}(N, c, \tau)}{\sqrt{2}\,\sigma_{\Delta H^{\text{sol}}}(c, \tau)} + \frac{\sigma_{\Delta H^{\text{sol}}}(c, \tau)}{\sqrt{2}\,kT} \right), \tag{9}$$

where $\Delta \overline{H}^{\text{sol}}$ is the largest reduction in activation energy among all the N segments (the "weakest-link", see below), k is Boltzmann's constant, ν_0 is an appropriate attempt frequency, and erfc is the complementary error function. In the absence of solutes, or for very weak solute/screw interactions, the nucleation rate is

$R = \nu_0 N \exp(-\frac{\Delta H^0(\tau)}{kT})$ which is the rate for a dislocation length in the pure matrix.

The temperature- and stress-dependent plastic shear strain rate $\dot{\epsilon}$ at applied stress τ then follows from Orowan's law as $\dot{\epsilon} \approx \rho b a R$, where ρ is the mobile dislocation density and R is the nucleation rate. Using this relationship, the yield stress as a function of temperature and strain rate can be determined, as described in more detail in the context of the applications presented in Section 5.

At sufficiently low temperatures, the rate of double-kink nucleation is controlled by that one segment having the greatest reduction of the kink-pair nucleation barrier; i.e. nucleation is an extreme-value (weak-link) problem. For a dislocation of length Nl_{dk}, the *mean* of the lowest activation energy is

$$\Delta \bar{H}^{\text{sol}} = \frac{\int_{-\infty}^{\infty} \cdots \int_{-\infty}^{X_3} \int_{-\infty}^{X_2} X_1 \prod_{n=1}^{N} P(X_n) \, dX_n}{\int_{-\infty}^{\infty} \cdots \int_{-\infty}^{X_3} \int_{-\infty}^{X_2} \prod_{n=1}^{N} P(X_n) \, dX_n}, \tag{10}$$

The standard deviation of activation energies around this mean lowest value is

$$\bar{\sigma}_{\Delta H^{\text{sol}}}^2 = \frac{\int_{-\infty}^{\infty} \cdots \int_{-\infty}^{X_3} \int_{-\infty}^{X_2} \left(X_1 - \Delta \bar{H}^{\text{sol}} \right)^2 \prod_{n=1}^{N} P(X_n) \, dX_n}{\int_{-\infty}^{\infty} \cdots \int_{-\infty}^{X_3} \int_{-\infty}^{X_2} \prod_{n=1}^{N} P(X_n) \, dX_n}, \tag{11}$$

For long lengths L, corresponding to large N and relevant for real physical systems, the above distributions are asymptotically approximated by the extreme-value Gumbel distribution having the cumulative probability

$$C_N(\Delta H^{\text{sol}}) \approx 1 - e^{-e^{\frac{\Delta H^{\text{sol}} - \sigma_{\Delta H^{\text{sol}}} b_N}{\sigma_{\Delta H^{\text{sol}}} a_N}}} \tag{12}$$

where the Gumbel scale a_N and location b_N parameters are

$$a_N = \frac{1}{\sqrt{2\log(N)}},$$
$$b_N = \frac{\log(\log(N)) + \log(4\pi)}{\sqrt{8\log(N)}} - \sqrt{2\log(N)}, \tag{13}$$

respectively. In terms of $\sigma_{\Delta H^{\text{sol}}}$, the mean and standard deviation at length Nl_{dk} are

$$\Delta \overline{H}^{\text{sol}}(c, N, \tau) = \sigma_{\Delta H^{\text{sol}}}(c, \tau)(b_N - \gamma \, a_N),$$
$$\overline{\sigma}_{\Delta H^{\text{sol}}}(c, N, \tau) = \sigma_{\Delta H^{\text{sol}}}(c, \tau)\frac{\pi}{\sqrt{6}}a_N, \tag{14}$$

where $\gamma \approx 0.5772$. Numerical tests show these asymptotic results to be quite accurate for $N > 15$ while exact results from Eqs. (10) and (11) can be computed for $N < 15$. One feature of the weak-link analysis is that the mean contribution of solutes increases with increasing N but the standard deviation decreases. Also, the temperature T_0 below which the weak-link dominates can be determined (see Appendix B) and the double-kink nucleation rate can be expressed as

$$R = \nu_0 \exp\left(-\frac{\Delta H^0(\tau) + \Delta \bar{H}^{\text{sol}}(c, N, \tau)}{kT} \right), \tag{15}$$

The weak-link limit provides an easy-to-use analytic form.

Eqs. (5), (6), and (8) together with Eq. (10) (for $N < 15$), and Eqs. (13) and (14) (for $N > 15$) constitute our analytic statistical model for the reduction in double-kink nucleation barrier due to solutes in the dilute limit. The only inputs to the theory are the matrix transition state shape versus stress, the solute/dislocation interaction energies, and the dislocation line length Nl_{dk}.
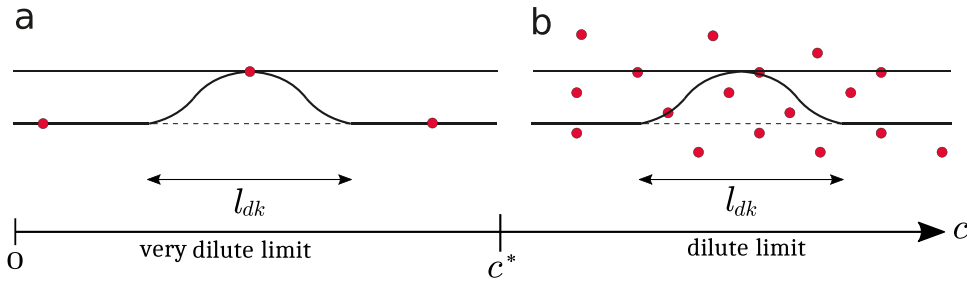
Fig. 4. Schematic of the solute (red dots) distribution surrounding a double-kink nucleation structure with length l_{dk} for (a) very dilute ($c < c^*$) and (b) dilute limit ($c > c^*$) cases. When $c < c^*$ there will be at most one solute within the length l_{dk}. Whereas, multiple solutes may be found within double kink nucleation length when $c > c^*$. (For interpretation of the references to colour in this figure legend, the reader is referred to the web version of this article.)

Lastly, the solute/double-kink interaction energies are modeled using the transition state configurations of the pure matrix at the relevant applied stress. However, a careful treatment is required at zero stress since the transition state in the pure metal is strictly equal to 1/2 the total simulated dislocation length. As shown below, even in the very dilute limit where the transition is affected only by one isolated solute, the transition state at zero stress is always localized around the position of a single favorable solute. The transition state structure is never that found in the pure material (spanning 1/2 the cell size). Therefore, here we use the transition state configuration at the lowest non-zero stress where the kinks are well-formed but only separated enough such that the leading part of the transition state is very nearly in the final-state Peierls valley. For our model system, this corresponds to the configuration at 0.1 GPa in Fig. 3. In all subsequent analyses, the transition state configuration at zero stress $x_{disl}(z_k, 0)$ refers to this configuration. This assumption enters the model only through the structure-dependent factor $G(0)$; any other approximation to the zero-stress transition state structure would simply correspond to a (small) change in the value of $G(0)$. We validate our zero-stress transition state structure via direct simulations for specific solute configurations in a model Fe-Si alloy in Section 4.2.

3. Solute effects in the very dilute limit

The previous analysis is valid for concentrations above a critical value in which multiple solutes are present across the double-kink nucleation length l_{dk} so that a statistical analysis is appropriate. In the very dilute limit, however, at most only a single solute will exist around the dislocation over length l_{dk} and its affect on the double-kink nucleation requires special treatment as discussed here.

Far from the screw dislocation core, the solute/dislocation interaction energy differences are vanishingly small and so do not affect the double-kink nucleation barrier. There are thus only some finite number of distinct atomic sites that contribute to the double-kink nucleation energy difference. We denote the number of atomic sites with appreciable negative interaction energy differences per unit b of line length as N_T. Due to symmetry, there are then also N_T sites with positive appreciable energy difference. A critical concentration is then defined as $c^* = b/(2N_T l_{dk})$, at which there exists, on average, only one solute among all the $2N_T$-type sites over the entire double-kink nucleation length l_{dk}. For concentrations above this critical concentration, multiple solutes are found within the double-kink nucleation length and the analysis of the previous section quickly becomes relevant. When $c < c^*$, there will be only one solute or no solute within each double-kink nucleation length. The concentration c^* is thus the boundary between the very dilute limit and the dilute limit cases (see Fig. 4).

In the very dilute limit, the change in interaction energy of a solute initially at the i-th distinct site ($i = 1, \ldots N_T$) due to motion

of the straight screw dislocation from the initial to the final is now labeled simply as ΔU_i. A dislocation of length L with $N = L/l_{dk}$ double-kink nucleation segments will have a fraction c/c^* of segments containing one solute randomly distributed among the $2N_T$ possibilities while the remaining fraction $(1 - c/c^*)$ of segments are solute-free. The latter fraction have a double-kink activation barrier ΔH^0 equal to that of the pure matrix. Nucleation will be preferred in segments containing solutes having favorable interaction energies, and nucleation will be centered on the solute position. Therefore, the barrier change due to a single favorable solute at site i is

$$\Delta H_i^{sol}(\tau) = \Delta U_i g(0, \tau).\tag{16}$$

The nucleation rate is slower in segments containing solutes with unfavorable interaction energies. As an approximation, we treat these segments as having zero solutes, which slightly overestimates the nucleation rate in these segments. The total double-kink nucleation rate R_{dk} is then the sum of the rates over all segments, with or without solutes,

$$R_{dk} = \underbrace{\sum_{k=1}^{(1-\frac{c}{c^*})N} \nu_0 \exp\left(-\frac{\Delta H_0(\tau)}{kT}\right)}_{\text{pure matrix}} + \underbrace{\sum_{k=1}^{(\frac{c}{c^*}N)/2} \nu_0 \exp\left(-\frac{\Delta H_0(\tau)}{kT}\right)}_{\substack{\text{segments containing}\\\text{one unfavorable solute}}}$$

$$+ \underbrace{\sum_{k=1}^{(\frac{c}{c^*}N)/2} \sum_{i \in N_T} \nu_0 s_i \exp\left(-\frac{\Delta H_0(\tau) + \Delta H_i^{sol}(\tau)}{kT}\right)}_{\substack{\text{segments containing}\\\text{one favorable solute}}},\tag{17}$$

where the summation over i extends over all N_T favorable sites and $s_i = 1$ for site i containing a favorable solute and $s_i = 0$ for all other sites. Noting that $\langle s_i \rangle = 1/N_T$ the above equation can be reduced to

$$R_{dk} = N\nu_0 \exp\left(-\frac{\Delta H_0(\tau)}{kT}\right)$$

$$\times \left[1 + c\frac{l_{dk}}{b} \sum_{i \in N_T} \left(\exp\left(-\frac{\Delta H_i^{sol}(\tau)}{kT}\right) - 1\right)\right].\tag{18}$$

Recall that N_T is the number of sites with appreciable negative interaction energy changes. The above relation shows that the inclusion of more-distant sites, i.e. those having comparatively low interaction energy changes compared to those within the N_T sites, will not influence the double-kink nucleation rate since $\exp(-\Delta U_i g(0, \tau)/kT) - 1 \approx 0$ for such sites. Thus, the choice of the N_T sites mainly affects the definition of the critical concentration c^* rather than the actual rate of nucleation in this domain.

The transition from the very dilute to the dilute limit is not fully developed. Neither result is quite correct at concentrations $c \sim c^*$: there will often be more than one solute with l_{dk} but not

quite enough such that the asymptotic random Gaussian statistics is applicable. However, the critical concentration $c^\star$ may be below commonly-studied solute concentrations of dilute BCC binary alloys (1 at.%). Therefore, a lack of precision in the definition of $c^\star$ and the behavior in the vicinity of $c^\star$ is not a major issue.

4. Validation against atomistic simulations using a model Fe-Si alloy

We now compare predictions of our analytical model for double-kink nucleation enthalpy barrier against direct atomistic simulations using a model Fe-Si alloy. The only input parameters to the model are the solute/screw-dislocation interaction energies $U(x_i, y_j)$ at all distinct solute positions ij around the screw core, the length L of the dislocation, and the stress-dependent enthalpy barrier and transition state dislocation configurations of the pure matrix material. There are no fitting parameters.

We use a model Fe-Si alloy system as represented by a recent EAM potential [2]. The Fe-Fe interactions are based on the Fe EAM potential developed by Proville et al. [19], which has all the key aspects for Fe screw dislocations such as the non-degenerate compact core structure, the single-hump Peierls potential, and {110} slip-plane. We further set the Si-Si interaction energies to those of Si-Fe, which eliminates direct solute-solute interactions. Since we are interested in dilute alloys and since the theory does not include solute-solute interactions, this treatment of solute-solute interactions is convenient and very useful. We note clearly that this Fe-Si potential is not an accurate representation of real Fe or real Fe-Si. However, it is a well-defined model system with no pathological behaviors that often plague atomistic modeling of BCC screw dislocations. Thus, this model Fe-Si system is well-suited to validate our general analytic model in detail.

The solute/screw dislocation interaction energy parameter $\Delta \tilde{E}_p(a)$ is computed using the individual solute/dislocation interaction energies shown in Fig. 2b. The individual energies were computed as discussed carefully in [23]. The resulting solute/dislocation interaction energy parameter for this model Fe-Si alloy is then computed as $\Delta \tilde{E}_p(a) = 344\sqrt{c}$ meV.

To compute the transition path from the initial to the final state, we use the nudged elastic band (NEB) method as implemented in LAMMPS. To find the minimum energy path (MEP) under applied shear stress, we followed the procedure outlined in [20]. Details of the NEB simulation can be found in Appendix C. NEB calculations on the pure Fe matrix at various stresses up to the Peierls stress $\tau_p \approx 1000$ were performed. The transition state configurations, determined using the disregistry method [22], are shown in Fig. 3. These configurations were fit to a functional form for $g(z, \tau)$ as

$$g(z, \tau) = \frac{1}{2}\left(\tanh\left[\frac{z/b + \zeta(\tau)}{\alpha(\tau)}\right] - \tanh\left[\frac{z/b - \zeta(\tau)}{\alpha(\tau)}\right]\right), \quad (19)$$

where $\zeta(\tau)$ and $\alpha(\tau)$ are two fitting parameters shown in Table 1. The kink-pair nucleation length was estimated as $l_{dk} = 20b$, consistent with the result of [2]. The initial positions $g_{eq}(\tau)$ and the geometrical shape factor $G(\tau)$ are shown in Table 1. The maximum energy along each energy path is the double-kink nucleation energy barrier $\Delta H^0(\tau)$ for pure Fe as described by this potential, which was fit to the empirical form $\Delta H^0(\tau) = (0.62\,\text{eV})(1 - (\tau/1000\,\text{MPa})^{0.62})^{1.02}$ for later use.

To study the (weak-link) scaling of the nucleation barrier with total dislocation length, NEB simulations are performed for lengths $40b$, $70b$, $100b$, and $200b$. The shortest length of $40b$ is the shortest length at which the double-kink nucleation barrier in pure Fe becomes essentially length-independent, i.e. at which there is very limited interaction between the two kinks formed during kink-pair nucleation. Specifically, the pure Fe enthalpy barrier at $40b$ is 572 meV, only 28 meV smaller than the value 600 meV at $200b$. NEB calculations are then performed to find the double-kink nucleation barrier in random Fe-Si dilute alloys for a range of stresses and solute concentrations of 1, 2, and 4%. At zero stress 200 different realizations of random Si are considered at each concentration while 120 cases are studied at non-zero stresses.

4.1. Very dilute limit: the single solute

NEB calculations of the double-kink nucleation process in the model Fe-Si alloy containing a single Si atom at 6 different atomic sites (numbered in Fig. 2f) were performed. The interaction energy changes upon glide range from -113 meV to -69 meV for these 6 sites. Fig. 5 shows the enthalpy barriers for double-kink nucleation barrier versus the applied stress τ for each solute position. Similar studies were performed by Shinzato et al. [2], which served as the only input into their subsequent Monte Carlo studies at all concentrations. All of these favorable sites reduce the pure double-kink nucleation barrier, with a decreasing effect with increasing applied stress. Also shown is the prediction for one particular case, site #4 with interaction energy change -89 meV. For each solute, the trends follow the model predictions (not shown except for site #4) in general, but the precise results do not agree exactly. The nucleation path adjusts very subtly to the precise solute position, affecting the energy barrier slightly, and this cannot be captured in the model. Across all these cases, the differences between NEB and model are roughly +/- 20 meV, which is comparable to the differences among the 6 solute interaction energies. This result sets a level of agreement that can be expected for subsequent results.

4.2. Validation of solute/double-kink interaction energies

In our model, the collective interaction energies of the solutes with the double-kink transition state (Eq. (3)) were modeled using the transition state configuration of the pure matrix at the relevant applied stress (Fig. 3) and an approximation for the solute/transition state interaction energies (Eq. (2)). Here, we test the model by comparing the predicted and NEB-computed *changes* in nucleation barrier $\Delta H^{sol}(0)$ due to *specific* arrangements of solutes at zero stress.

Si solute configurations were created by placing multiple Si solutes at selected atomic sites around the dislocation core. The configurations were selected so as to sample various local energy environments (combinations of solute positions, including favorable and unfavorable sites, at different distances). The configurations used are shown schematically in see Fig. 6(a), with solutes labeled by the atomic row (1–8 as indicated in Fig. 2e) and with an additional overbar notation for multiple solutes spaced along the same row. The spacings of solutes along the same row are indicated by either w or d, as shown in the figure. For each specific set of solute positions, we calculated the double-kink nucleation barrier change at zero stress using Eq. (3) and the transition state shape parameter $G(0) = 3.07$ shown in Table 1. Direct NEB calculations were performed on the exact same solute configurations at zero applied stress.

The atomistic and predicted results for the change in nucleation barrier are shown in Fig. 6(b). The trends in the simulation are well-predicted by the analytic model with no adjustable parameters. The generally good agreement between the predicted and simulated energy changes for most of the cases (deviating by only 20–30 meV except for one extreme case discussed below) shows that the use of the zero stress transition state structure to describe the collective effect of multiple solute/double-kink interaction energies is quite accurate. The maximum deviation in Fig. 6(b) is for the case $1 + \bar{1} + 5 + \bar{\bar{5}}, d = 3b$. However, this configuration consists of solutes in four energetically-favorable positions, two of which
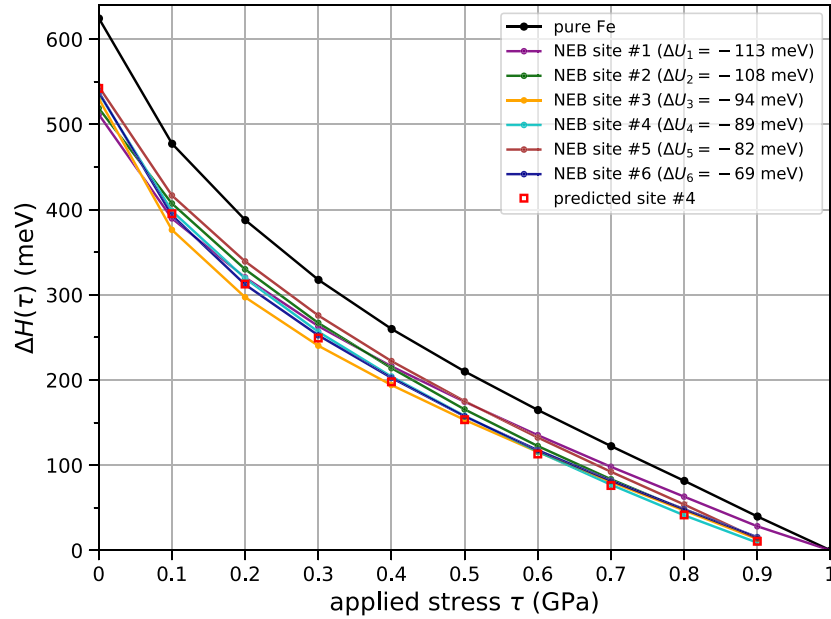
Fig. 5. The double-kink nucleation enthalpy barriers, $\Delta H(\tau)$ versus the applied stresses τ for various single Si positions in Fe matrix. The solute/screw interaction energy change associated with each site, ΔU_i is also shown.
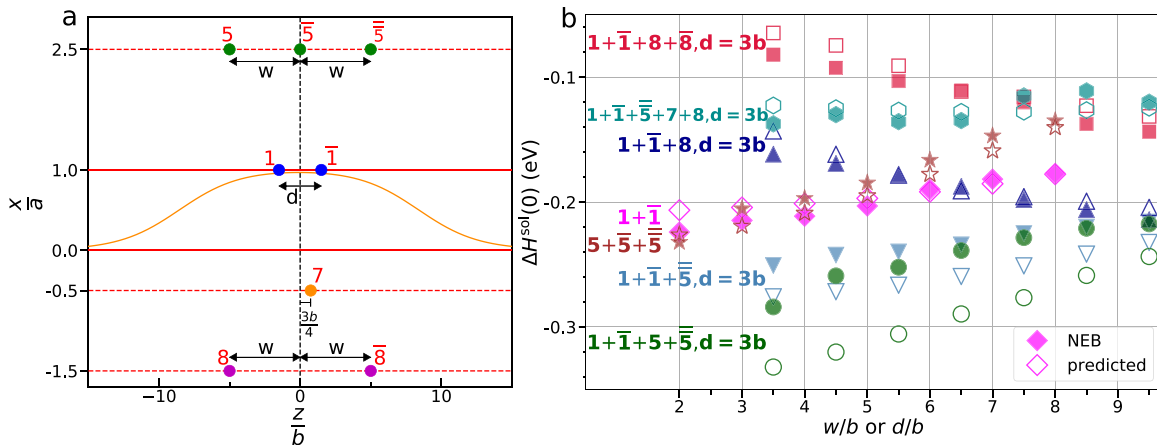

Fig. 6. (a) Definition of solute positions relative to a double-kink nucleation shape (orange solid line). Same color and number is used for solutes in a same atomic row position (x_i, y_j) consistent with sites marked in Fig. 2f. (b) The zero stress double-kink nucleation enthalpy barrier changes $\Delta H^{sol}(0)$ due to different solute combinations. The numbers indicate the numbered solutes in (a); e.g. $1 + \overline{1} + 8, d = 3b$ denotes solutes at sites #1 and #$\overline{1}$ at fixed distance $d = 3b$ plus a solute at site #8 at various w distances. (For interpretation of the references to colour in this figure legend, the reader is referred to the web version of this article.)

are in the most favorable positions, and no other solutes. This is thus an extreme case - all the solutes are strongly attracting the double-kink - that is very unlikely to occur in the dilute alloys. Evidently, it distorts the transition state shape away from the assumed shape sufficiently to reduce the effect of the solutes. Overall, however, while the precise double-kink transition state structure in the NEB varies with each distinct solute configuration, with solutes pulling/pushing the dislocation line away from the pure Fe shape, our model remains quite good, and so is a quantitative parameter-free analytical model.

4.3. Double-kink nucleation in model dilute Fe-Si random alloys

Finally, we compare our predictions of the double-kink nucleation barrier for the model binary random Fe-Si dilute alloys to direct NEB simulations for a range of solute concentrations and dislocation lengths and under zero and non-zero stresses. The NEB selects the lowest barrier in any particular realization, and so our predictions use the weakest-link limit (Eq. (10)) appropriate for the NEB simulations.

4.3.1. zero stress

Fig. 7(a)–(d) show the mean, statistical distribution, and standard deviation of the NEB double-kink nucleation barrier ΔH as a function of solute concentration for dislocation lengths $L = 40b, 70b, 100b$, and $200b$, respectively, at zero stress. The corresponding predictions of the theory for the mean and standard deviation, with no adjustable parameters, are also shown. As predicted, the changes in nucleation energy barrier are statistically-distributed in random dilute alloys and are a function of both solute concentration and dislocation length.

At the shortest length of $40b$, there is essentially no weak-link scaling effect. The distribution of barriers is centered on the single-solute result, not the zero-solute result, because the nucleation will typically occur around the single most-favorable solute. The standard deviation, which is representative of the statistical variations from sample to sample, increases as the concentration
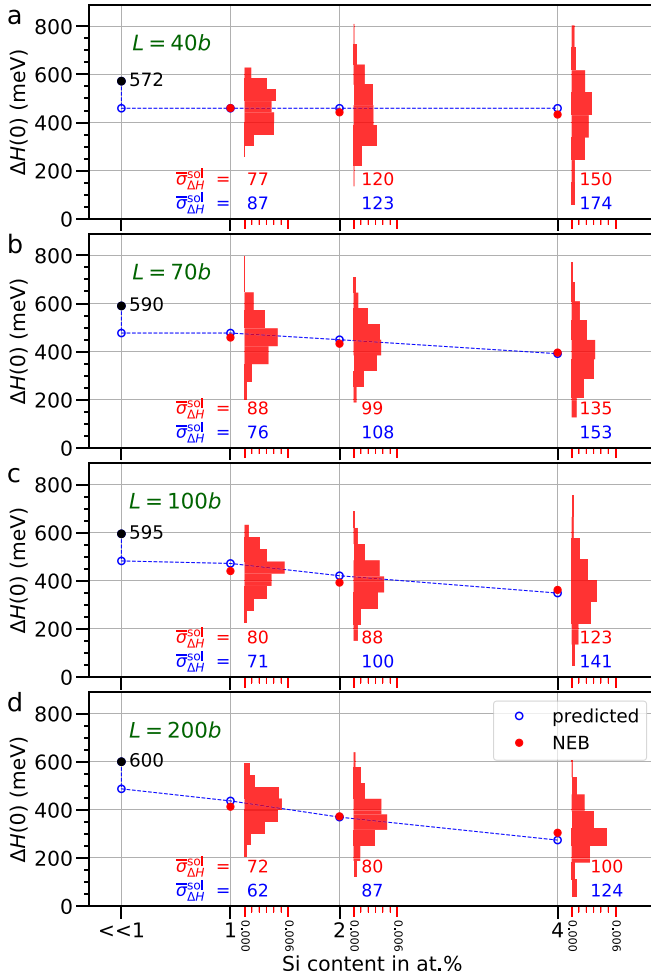
Fig. 7. Zero stress double-kink nucleation barrier $\Delta H(0)$ versus solute concentration c for dislocations with length L (a) $40b$, (b) $70b$, (c) $100b$, and (d) $200b$. The histograms show the distribution of double-kink nucleation barriers obtained by NEB calculations. The black numbers are the enthalpy barriers for double-kink nucleation in no solute pure Fe. The red and blue numbers are the standard deviations of the distributions of double-kink nucleation barrier obtained by NEB simulations and theory, respectively. (For interpretation of the references to colour in this figure legend, the reader is referred to the web version of this article.)

increases. The theory predicts both the mean and standard deviation in good agreement with the simulations, with no adjustable parameters. The results at $40b$ represent the "unit" statistical process, with weak-link length effects entering for longer lengths.

For the longer lengths $70b - 200b$, the mean barrier decreases because the system can find the weakest among several possible nucleation environments along the dislocation line, as predicted by the theory. The standard deviation also narrows slowly, as predicted. All the trends predicted by the theory agree quantitatively with the simulations. At length $200b$, essentially none of the simulations at 1, 2 or 4% has a barrier that exceeds that of pure Fe. The system always finds some favorable solute fluctuations that reduce the double-kink nucleation barrier, i.e. "softening" the alloy, even at this rather small dislocation length. Note that these results are for double-kink nucleation only; kink migration is not investigated even though it may become the rate-controlling factor at higher concentrations.

4.3.2. Non-zero stress

The predictive model is further verified by comparing to NEB simulations under applied stresses in the range 100–900 MPa. Simulations were performed for a single dislocation length of $70b$

and concentration of 2%. Fig. 8 shows the mean enthalpy barrier as simulated and as predicted, along with the enthalpy barrier for pure Fe. The statistical distribution of barriers as simulated is shown as a histogram and is important because nucleation in realistic systems will occur along lengths much larger than $70b$.

Very good agreement is found between the predicted and NEB results. The barrier reduces as the stress increases, but the difference between pure Fe and the alloy decreases with increasing stress. At a stress of 70% of the Peierls stress, the spectrum of barriers extends to zero (and below). That is, for some cases, the initial dislocation position is unstable (zero barrier) against gliding forward into the lower-energy state in the next adjacent Peierls valley. These cases are not shown and the predictions for the mean barrier at the higher stresses must use a lower limit of $-\Delta H^0(\tau)$ in the integrals in Eq. (10). More importantly, for longer lengths, the mean barrier at any stress will decrease even further, with the standard deviation decreasing only slowly, enabling zero-energy barriers to occur with increasing frequency.

The results in Fig. 8 fully validate our analytic model for double-kink nucleation in random alloys as a function of both concentration and stress. For any length dislocation beyond more than a few segments, and at all stresses below the Peierls stress, the presence of solutes reduces the double-kink nucleation barrier, i.e. solutes always soften double-kink nucleation. This validation is performed on a model Fe-Si alloy where all material parameters are known, but now enables application of the analytic model to be applied to realistic alloys using input material parameters relevant for the real alloys.

5. Applications and implications

The agreement between theory and simulation shown in the previous section on a model random dilute Fe-Si alloy validates all of the major features of the theory, and demonstrates the quantitative accuracy of the approximations that render the theory analytic. The theory can thus be applied with confidence to any bcc alloy system in the dilute limit. Challenges in applying the theory lie in obtaining accurate input data and also accurate experimental results. Nonetheless, below we achieve some insights in making comparisons to experiments at a level of detail well beyond previous literature.

We first address how the theory can be used to estimate the yield strength of a dilute alloy. The material parameters in the theory are reiterated: (i) the double-kink nucleation barrier and transition state configurations of the pure matrix; (ii) the double-kink nucleation length and total dislocation length; and (iii) the solute/screw dislocation interaction energies. The interaction energies can in principle be computed using first-principles (e.g. Fig. 2(a) and (c)), although this is computationally challenging and still not necessarily precise for the real material. The double-kink nucleation length can be estimated reasonably by various means [18,20]. The stress-dependent double-kink nucleation barrier for the pure matrix is derived from experiments of the flow stress versus temperature as explained below.

Obtaining $\Delta H^0(\tau)$ from experiments requires accounting for the number of nucleation sites N along each dislocation segment of length $L = 1/\sqrt{\rho}$ between dislocation junctions. When deformed at a constant strain rate $\dot{\epsilon}$, the thermally-activated Arrhenius model plus the Orowan model leads to a strain rate $\dot{\epsilon} = N\rho b a v_0 \exp(-\Delta H^0(\tau)/kT)$ where $N \sim 1/(l_{dk}\sqrt{\rho})$ is the number of possible nucleation sites along dislocations in between dislocation junctions. A reference strain rate $\dot{\epsilon}_0$ often replaces the combination $\rho b a v_0$. The enthalpy barrier at stress τ is then obtained as

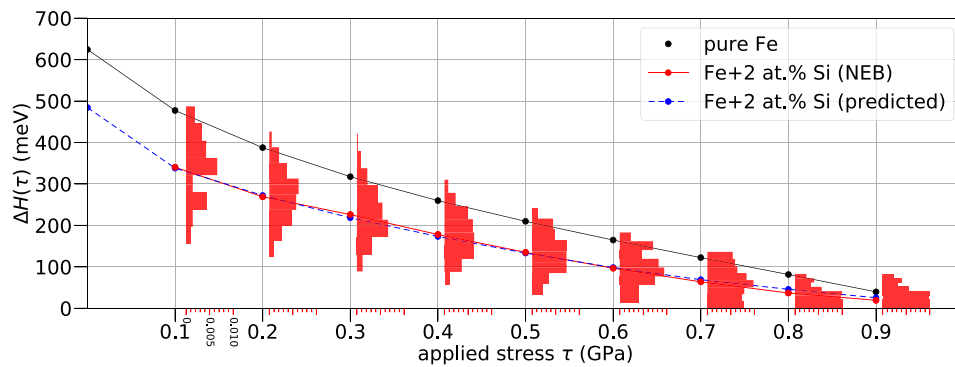$$\Delta H^0(\tau) = \Delta H^0_{exp}(\tau) + kT \log(N). \tag{20}$$

Fig. 8. The double-kink nucleation barrier $\Delta H(\tau)$ versus applied stress τ for dislocations with length $L = 70b$ in Fe-2at%Si dilute alloys. The histograms are the distribution of double-kink nucleation barriers obtained by NEB atomistic calculations.
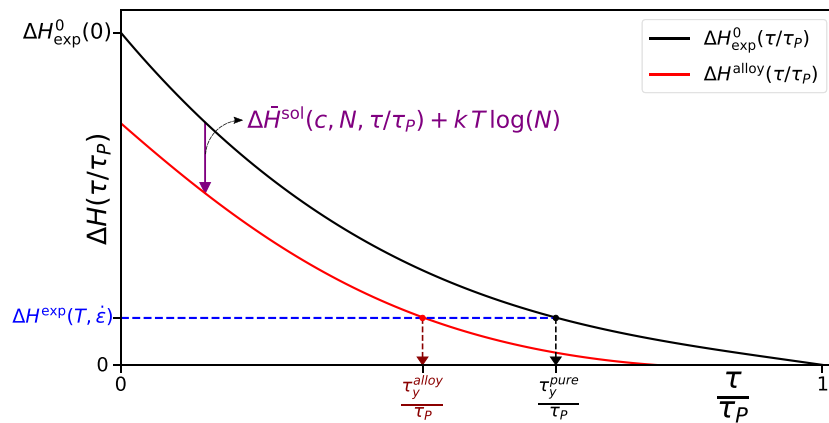

Fig. 9. Generic prediction of solute softening by double-kink nucleation starting from double-kink nucleation in the pure metal. The experimental barrier versus stress must first be corrected for the number of nucleation segments N, and then the additional effect of softening is added to obtain the total activation enthalpy. At a given experimentally-imposed activation enthalpy determined by the temperature and strain rate, the alloy has a lower yield stress than the pure metal. The example here uses the weak-link limit for illustration.

where $\Delta H^0_{exp}(\tau) = kT \log(\dot{\epsilon}_0/\dot{\epsilon})$ is the experimental enthalpy barrier obtained from the experimental flow stress versus temperature experimental data.

With the above details, softening by solutes is then determined as shown schematically in Fig. 9. Starting with the experimental enthalpy barrier versus stress, the correction is made for N, and then the contribution of the solutes is added, where the figure shows the case where the low-temperature weak-link result is applicable. An experiment carried out at a particular $\Delta H^{exp} = kT \log(\dot{\epsilon}_0/\dot{\epsilon})$ determined by the specified temperature and strain-rate will then measure the strengths indicated in Fig. 9.

While the weak-link analysis can only be applied for low temperatures $T < T_0$, the total nucleation rate due to all nucleation sites, Eq. (9), can be applied for the whole temperature range of interest. In this case, considering Eq. (20) along with Orowan's law, Eq. (9) is solved numerically to determine the yield stress at a given strain rate and temperature. In the following, the full rate theory has been used to predict the yield stress of real dilute Fe-Si, W-Re, and W-Ta alloys.

5.1. Application to Fe-Si alloys

We now use the theory to make specific predictions for real dilute Fe-Si (0.52 at%, 1.3 at%, 3.2 at%, and 5 at%) alloys over a wide temperature range and compare to the experimental data of [24] performed at a strain rate of $1.7 \times 10^{-4}\,\mathrm{s}^{-1}$. We use a reference strain rate of $10^4\,\mathrm{s}^{-1}$ and take a dislocation density of $\rho = 10^{12}\,\mathrm{m}^2$ ($L \sim 1\mu\mathrm{m}$; $N \sim 170$) based on the TEM measurements of Takeuchi [25].

The same Fe-Si alloys at 5 at% and higher were previously studied by Maresca and Curtin [16] using the non-dilute theory. There is significant strengthening at this concentration, indicating that the non-dilute theory is appropriate. Good agreement in strength versus temperature at these higher concentrations was obtained using a solute/dislocation interaction energy parameter $\Delta \tilde{E}_p = 178\sqrt{c}$ meV, and so we use this value here. The transition state configurations for pure Fe are taken from a study using a machine-learning interatomic potential trained on a very large DFT dataset [20] with double-kink nucleation length $l_{dk} = 12\,b$. Both the interaction energy parameter and the double-kink transition state structures differ from those of the model Fe-Si EAM potential precisely because that potential is not quantitative for real Fe-Si.

Our predictions are shown in Fig. 10. For 0.52at%Si at low T, the experiments show a very small hardening while the theory predicts a very small amount of softening. At higher T > 200K, the prediction and experiment are similar, and deviations from pure Fe are quite small. There is a small hump in the data around 150K, widely discussed but unexplained to date [26–28]. For the 1.3at%Si alloy, there is again a very small strengthening seen at low T and minimal effects at higher T. The predictions show a small softening at low T and then little net effect at higher T. For 3.2at%Si, at low T there is slight softening and then a small but distinct strengthening at higher T > 100K. The theory shows a stronger softening that remains roughly constant relative to pure Fe over the entire temperature range. At 3.2at%Si, the double-kink nucleation theory deviates significantly from experiments throughout the entire temperature regime, suggesting another mechanism controlling deformation (see below). Further significant deviations
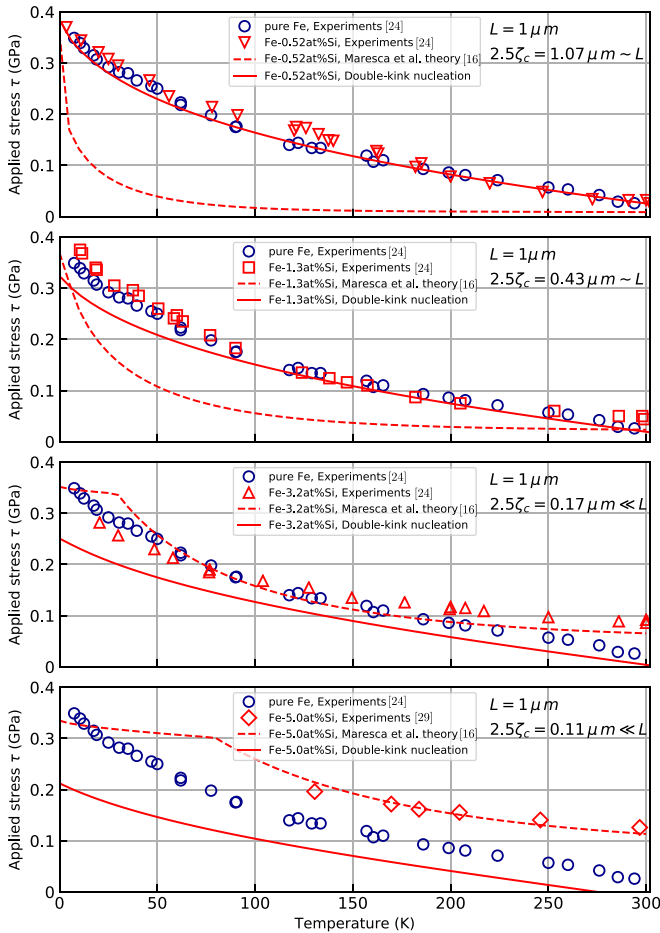
Fig. 10. Theory predictions for $Fe_{1-x}Si_x$ alloys [29].

the spontaneous kinks. If this length is smaller than the distance L between forest junctions, then the Maresca et al. model should apply and the alloy is in the non-dilute regime. If the kink spacing is predicted to be larger than L, then the spontaneous kinked structure cannot actually form, and thermally-activated double-kink nucleation is necessary; such alloys are in the dilute regime where the present theory should apply. Maresca et al. predict the spontaneous energy-minimizing kink-spacing to be $2.5\,\zeta_c$ where $\zeta_c = (1.083 E_k/\Delta \tilde{E}_p)^2 b$ is a critical length scale that depends only on the ratio between the kink formation energy ($E_k = 0.5\,\Delta H^0(0)$) and the solute/dislocation energy quantity $\Delta \tilde{E}_p$. The length scale $2.5\,\zeta_c$ that determines the boundary between dilute and non-dilute domains thus depends on precisely the two major material quantities that enter into the present double-kink nucleation theory ($\Delta H^0(0), \Delta \tilde{E}_p$). This enables direct comparisons of the two theories with no additional material parameters.

The legend in Fig. 10 shows the predictions of Maresca et al. for the length scale $2.5\,\zeta_c$ at each Si concentration. At both 0.52at%Si and 1.3at%Si, the length scale $2.5\,\zeta_c$ is larger than or comparable to L. According to our criterion, these alloys are thus expected to be in the "dilute" regime where double-kink nucleation controls the strengthening. This conclusion is supported by the reasonable agreement of the strength predictions using the double-kink nucleation theory and the poor agreement of the strength predictions (too low) of the Maresca et al. theory as shown in Fig. 10. In contrast, at 3.2at%Si, the length scale $2.5\,\zeta_c$ is definitely smaller than L and, correspondingly, the strength predictions of Maresca et al. are in fairly good agreement with experiments, aside from a small over-prediction at low $T < 75K$. At this concentration, the double-kink nucleation prediction is too low at all temperatures. The experiments at 5at%Si with $2.5\,\zeta_c \ll L$ are then, as expected, captured well by the Maresca et al. model while the double-kink nucleation model predictions are poor. This analysis supports a transition from the dilute softening regime to the non-dilute strengthening regime between 1.3at% and 3.2at%.

The transition here is based on temperature-independent length scales. The experiments at 3.2at%Si suggest that there can be both softening at low T and strengthening at higher T. The trends in strength versus temperature of the two different models also suggests that at concentrations in between 1.3at% and 3.2at% there could changes in the strongest mechanism vs. temperature. Such details are well beyond the scope of the present models.

Our predictions for Fe-Si can be further compared to experiments of Chen et al. [30] who reported the yield stress of dilute Fe-1at%Si and Fe-4at%Si polycrystals. Chen et al. converted the uniaxial polycrystalline yield stresses to critical resolved shear stresses (CRSS) by using the Taylor factor ~ 2.75 for bcc pencil glide. The resulting CRSS for pure Fe was then approximately 20% higher than that of Ref[24]., indicating the possibility that the data of Ref. [24] on pure Fe is low (for unknown reasons) which then brings into question the apparent strengthening at 0.52at%Si relative to the pure Fe data of Kitajima et al. More importantly, Chen et al. report distinct softening in Fe-1at%Si relative to pure Fe, in contrast to the results of Ref. [24] at 1.3at%Si. These comparisons demonstrate uncertainty in the pure and dilute Fe-Si data, which then leads to uncertainty in assessing softening versus strengthening.

To apply our analysis to the data of Chen et al., we must first shift the results of Chen et al. because our analysis was based on the pure Fe of Ref. [24] as a reference. To do so, we simply rescale all the data of Chen et al. by a single factor of 0.8 to best-match the pure Fe experimental data of Kitajima et al. We then make predictions for Fe-1at%Si as shown in Fig. 11. For 1at%Si, both experiments and theory show slight softening up to T=225K. The experiments then show a slight strengthening at T=300K that is not captured by the theory. The length scale $2.5\,\zeta_c$ and the strengthening predicted by Maresca et al. are also shown in Fig. 11. At
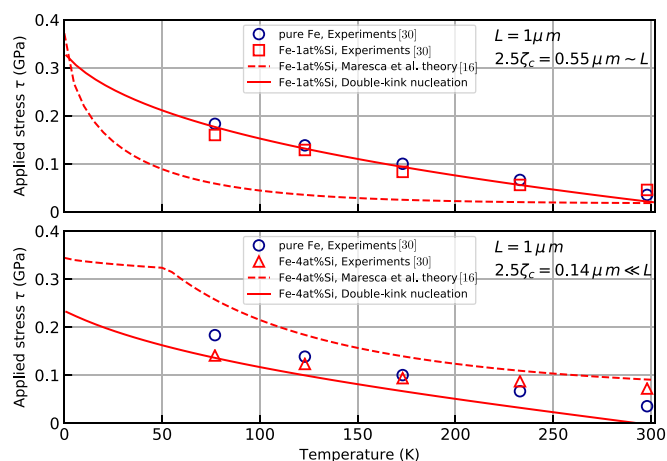
are obtained at an even higher concentration of 5at%Si, where the alloy is significantly strengthened but the double-kink nucleation theory predicts a large softening, relative to pure Fe, again indicative of another controlling mechanism (see below). The observed strengthening at low T for 0.52at%Si and 1.3at%Si is small and not explained by the present model. However, we show below another set of data at 1.0at%Si that shows distinct softening relative to pure Fe. Thus, the theory is qualitatively consistent with experiments at low concentrations in showing little effect of the solutes while the experiments themselves are in some conflict.

The failure of the present double-kink nucleation theory in comparison to the experiments at 3.2at%Si and higher concentrations is attributed to a transition from nucleation controlled softening at lower concentrations to some strengthening mechanisms at the higher concentrations. The traditional view is a transition to strengthening controlled by kink migration [1–3,6]. Here we apply the non-dilute yield strength model of Maresca et al. [16] that has successfully captured strengths in a number of bcc alloys. In this theory, an initially-straight screw dislocation in a random alloy lowers its energy by spontaneously forming a multiply-kinked structure at zero stress. The strength is then controlled by a combination of kink glide and cross-kink (also called jog or dipole) pinning, with a Peierls-like mechanism replacing kink glide at very low T. Crucially, there is no role of thermally-activated nucleation of double-kinks in this model, and so it is applicable only in the non-dilute regime.

The transition between dilute (double-kink nucleation controlled softening) and non-dilute (kink glide and cross-kink controlled strengthening) is then mainly dictated by the spacing of

Fig. 11. Theory predictions for $Fe_{1-x}Si_x$ alloys.

1at%Si, the predicted strengthening is well below the experiments at all temperatures and the length scale $2.5\zeta_c$ is comparable to L. These results indicate that this alloy is in the 'dilute' regime where double-kink nucleation controls the screw dislocation motion. This is consistent with our conclusions based on the data of Kitajima et al.

Similar predictions for Fe-4at%Si are shown in Fig. 11. At $T = 77$K, the experiments show a notable softening followed by a transition to strengthening above 200K. The length scale $2.5\zeta_c$ of Maresca et al. indicates this alloy should be in the non-dilute regime. In addition, the non-dilute theory captures the strengthening reasonably well at the higher temperatures. The double-kink nucleation theory is in good agreement with the experiments at low T, which is surprising since we would expect this alloy to be in the non-dilute regime. This suggests some temperature dependence to the dilute/non-dilute regime that is currently beyond the scope of the present analysis.

In spite of uncertainties in the experimental data, our analysis of the classic Fe-Si alloy provides a solid conceptual understanding of the nature of the transition in strengthening with increasing concentration. At low concentrations, there is generally softening by double-kink nucleation. At high concentrations, double-kinks are pre-existing and strength is controlled by kink migration and cross-kink formation. The transition is formulated in terms of length scales only, however. So, at concentrations in the transition range between 1.3 and 4 at%Si, strengthening may be a complex and temperature-dependent interplay between the two mechanisms. Such an interplay could be revealed by detailed kinetic Monte Carlo studies on long dislocation lengths that account carefully for the origins of kinks (pre-existing versus nucleating) and using the full statistical analyses for solute/screw interactions developed here. Existing kMC methods have already shown a transition generically, but have made simplifying assumptions about the solute/screw interactions, the kink formation, and the initial structure of the dislocation [2,3,31], that can perhaps be revisited.

5.2. Application to W-Ta and W-Re alloys

We now examine the yield stress for W-Re and W-Ta alloys at 0 (pure W), 1, and 3 at%, and temperatures $T = 150\,K$, $T = 300\,K$, and $T = 590\,K$. Experimental data was reported by Stephens [7] at a strain rate of $5.5 \times 10^{-4}\,s^{-1}$. We use the pure W data to estimate the pure W enthalpy barrier versus stress assuming the reference strain rate $\dot{\epsilon}_0 = 10^4\,s^{-1}$ and fitting a Kocks law as $\Delta H_{exp}^0(\tau) = \Delta H_{exp}^0(0)(1 - (\frac{\tau}{\tau_P})^{0.49})^{1.69}$ with $\Delta H_{exp}^0(0) = 1.4$ eV and $\tau_P = 1.1$ GPa. We use the transition state configurations obtained by GAP

for pure Fe, since estimates for W are similar [18]. We use the solute/dislocation interaction energies obtained by DFT (Fig. 2) from which we compute the solute/dislocation interaction energy parameters as $\Delta \tilde{E}_p = 345\sqrt{c}$ meV for W-Re and $\Delta \tilde{E}_p = 137\sqrt{c}$ meV for W-Ta. We again use a mobile dislocation density of $\rho = 10^{12}$ m^{-2} corresponding to $L = 1\,\mu$m and $N \sim 150$ segments along the length L when considering the transition to the non-dilute limit. We note clearly that, given the limited data to fit H_{exp}^0 and the uncertainty of other parameters, our predictions below are mainly qualitative and illustrative.

Predictions of the strength using the double-kink nucleation theory for the W-Re alloys are shown in Fig. 12(a). The predicted softening for W-1at%Re is in reasonable agreement with the experiments at all three temperatures. For W-3at%Re, the predicted softening increases, as expected, while the experiments at 150K and 500K show a slight strengthening relative to 1at%Re and the experiments at 300K exhibit continued softening. This suggests a mechanism transition between 1at%Re and 3at%Re. We thus evaluate the length scale $2.5\zeta_c$ of the Maresca model to assess a possible transition 3at%Re. Using the kink energy $E_k = 0.905$ eV from the DFT-based GAP potential for W [32], we predicted $2.5\zeta_c = 0.55\,\mu$m for W-1at%Re. This is comparable to the (approximate) dislocation length L, indicating that W-1at%Re is in the dilute regime. In contrast, we predict $2.5\zeta_c = 0.18\,\mu$m at 3at%Re, which is rather smaller than the (approximate) dislocation length L, suggesting that 3at%Re is in the non-dilute regime. The underpredictions of strength by the double-kink nucleation model at 3at%Re are thus qualitatively understood as being due to a transition to the non-dilute limit. The Maresca et al. model does not predicted a temperature-dependence of $2.5\zeta_c$ and so the observed softening at T=300K in W-3at%Re requires a full application of the Maresca et al. model before further conclusions can be made.

Both trends and uncertainties in the experiments on W-Re are revealed by examining the data of Raffo [33] on very clean polycrystals at 0, 1, and 2at% at temperatures of 77K, 298K, and 589K. Data at 77K (not shown) shows a steady softening, although very small at 1at%; there is no comparable data by Stephens. At T=298K, as shown in Fig. 12a scaled by the Taylor factor 2.71, Raffo shows a small strengthening at 1at%Re followed by softening at 2at% (but still stronger than pure W). At T=589K, as shown in Fig. 12a, there is softening at 1at% and strengthening at 2at%. If the single data point for pure W at T=298K were higher, the Raffo data would be qualitatively similar to the data of Stephens, and generally consistent with our analysis. Raffo also showed data at 7at% indicating continued softening at 77K but continued strengthening at 298K and 589K, the latter two results consistent with our analysis.

Predictions of the strength using the double-kink nucleation theory for the W-Ta alloys are shown in Fig. 12 (b). The experiments on W-Ta show a softening at 1at%Ta for all three temperatures studied. The double-kink nucleation theory predicts only a very slight softening for the 1at%Ta alloys, and so agrees only qualitatively with the experiments. The experiments at 3at%Ta show a slight strengthening at all three temperatures. The double-kink nucleation theory predicts continued softening, suggesting a transition in mechanism between 1 and 3at%Ta. However, the non-dilute theory of Maresca et al. predicts a length scale of $2.5\zeta_c = 1.1\,\mu$m at 3at%Ta that remains comparable to the (assumed) L and so does not quite indicate a transition at this composition. A transition would be expected only at slightly higher Ta content.

Overall, softening at 1at% is predicted and observed for both Re and Ta solutes, supporting the general concept that softening arises for all solutes. A transition to hardening at 3at% is captured by our analysis for Re but not for Ta. These findings remain tentative on both theoretical and experimental sides. The material parameters needed for the theory are estimated to the best of current ability
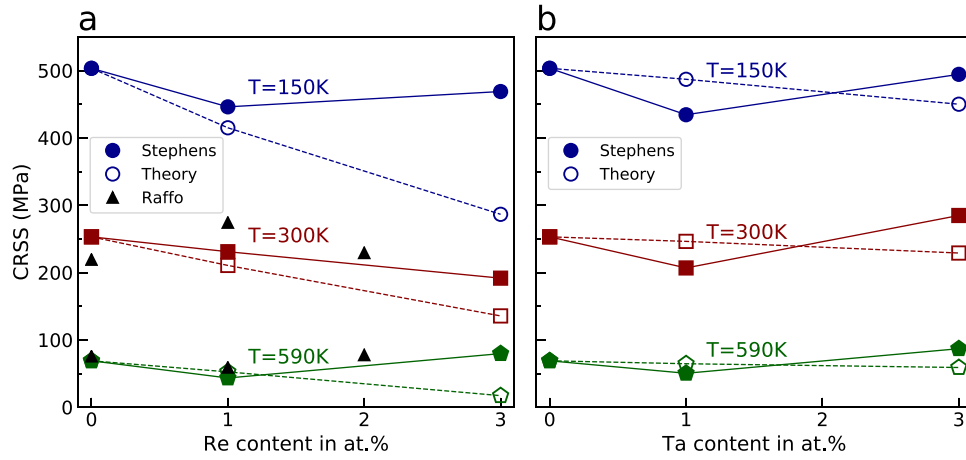
Fig. 12. Critical resolved shear stress (CRSS) versus solute concentration at various temperatures as indicated for (a) W-Re (filled symbols: data from Stephens [7]; open symbols: present theory; black triangles: data from Raffo [33]); (b) W-Ta (filled symbols: data from Stephens [7]; open symbols: present theory) dilute alloys.

but remain uncertain. In addition, it is not expected that there is a distinct transition from softening to hardening at some very specific concentration but rather a delicate and possibly temperature-dependent interplay of mechanisms. Identifying a precise transition is also not of practical importance - what is important is that the operative physical mechanisms be identified and quantified so that alloy design can proceed on the basis of these mechanisms. Even with these significant caveats, the two theories together (present theory and Maresca et al. theory) remain broadly consistent with the experiments and so provide the desired framework for alloy design.

We conclude with some remarks about previous modeling and simulation on the W-Re and W-Ta alloys. In the Introduction, we already discussed theoretical/conceptual issues with the model of Hu et al., and now focus on predictions. The model of [8] was applied to W-Re but was compared to hardness data at T=298K. Hardness and yield strength are not directly related, unfortunately, because hardness depends on the work hardening rate as well as the yield strength. This is clearly seen in the differences in flow stress versus solute type as a function of plastic strain in the uniaxial data of Stephens. Conclusions about relative softening and hardening based on experiments at a few percent plastic strain are thus inconsistent with the actual data at the onset of yielding. Hu et al. nonetheless converted the hardness data of Stephens and Witke at 298K [34] to a CRSS, leading to a CRSS for pure W of ~ 350 MPa significantly higher then the ~ 250 MPa reported by Stephens in direct uniaxial single crystal experiments. Hence, quantitatively, the predictions of Hu et al. do not agree with the uniaxial data of either Stephens or Raffo. The trends in converted hardness data do, however, suggest softening up to 5at%Re at T=298K while the uniaxial data of both Stephens and Raffo also indicate softening up to at least 2-3at%Re at T=298K. The uniaxial data, however, shows hardening at 3at%Re at both 150K and 590K, suggesting an underlying transition around 3at%Re that might not be predicted by the Hu et al. model. Zhao et al. [3] compared results from Monte Carlo studies to the data of Stephens at 2% plastic strain rather than to the data reported at yield, and these results differ. Zhao et al. also calibrated the pure W parameters in the Monte Carlo model to DFT results that are well-established to greatly overestimate the yield strength. Thus, the quantitative results of Zhao et al. are far higher than the experiments at both yield and 2% plastic strain. Examining trends only, Zhao et al. predict slight softening relative to pure W up to 5at%Re at 150K, in conflict with the experimental hardening at 3at%Re. They also predict essentially no softening at T=300K up to 1.5at%Re and very slight strengthening up to 5at%Re, again in

conflict with the distinct softening observed experimentally up to 3at%Re. At T=590K, Zhao et al. show a trend in good agreement with experiments. Overall, the results of Zhao et al. are quantitatively far from experiments and the trends are inconsistent with experiments. Finally, as noted in the Introduction, the model of Hu et al. was also applied to W-Ta and predicted strengthening, inconsistent with the softening data of Stephens.

5.3. Implications for spontaneous kinking in the non-dilute regime

The present theory is developed for understanding the softening in dilute alloys where double-kink nucleation controls the strengthening. However, the analysis of the effects of solutes on the double-kink nucleation barrier remains applicable to non-dilute alloys even though strength is not controlled by this mechanism. Recall that, in the non-dilute screw strengthening theory of Maresca et al., the initial straight dislocation in the random alloy at zero stress is spontaneously kinked at a characteristic length of $2.5\zeta_c$. Envisioning that the system is somehow prepared with initially-straight dislocations, the present analysis is applied to examine what barriers must be overcome to achieve the spontaneously-kinked length. This was not addressed in Maresca et al., where it was assumed that there is sufficient time to overcome such barriers in any real systems. Here, we can use the present analysis to examine the typical reduction in double kink nucleation barrier due to solutes over the characteristic length of ζ_c. The reduction in barrier then corresponds to a reduction in the average time required for the dislocation to attain the fully-kinked configuration envisioned by Maresca et al.

The relevant solute/screw interaction energy is a generalization of the dilute limit of Eq. (7) in which all elements of the alloy are considered to be solutes within an effective or average alloy matrix (see Maresca et al. and Ref. [23] for details). The interaction parameter is then $\Delta\tilde{E}_p = \left(\sum_{i,j}\sum_n c_n \Delta U_{ij}^{n\,2}\right)^{1/2}$ where the ΔU_{ij}^n is the energy change for a solute of type-n at initial position ij relative to a screw dislocation in the effective or average alloy material. This interaction parameter has been estimated for various HEAs in Maresca et al. and has been examined for a wide range of alloys described by interatomic potetntials by Ghafarollahi et al. [23]. Below, we use the values previously reported by Maresca et al. as shown in Table 2.

For simplicity, we assume a single double-kink nucleation length $l_{dk} = 20\,b$ for all of these non-dilute complex alloys. Based on the number of possible nucleation segments over each
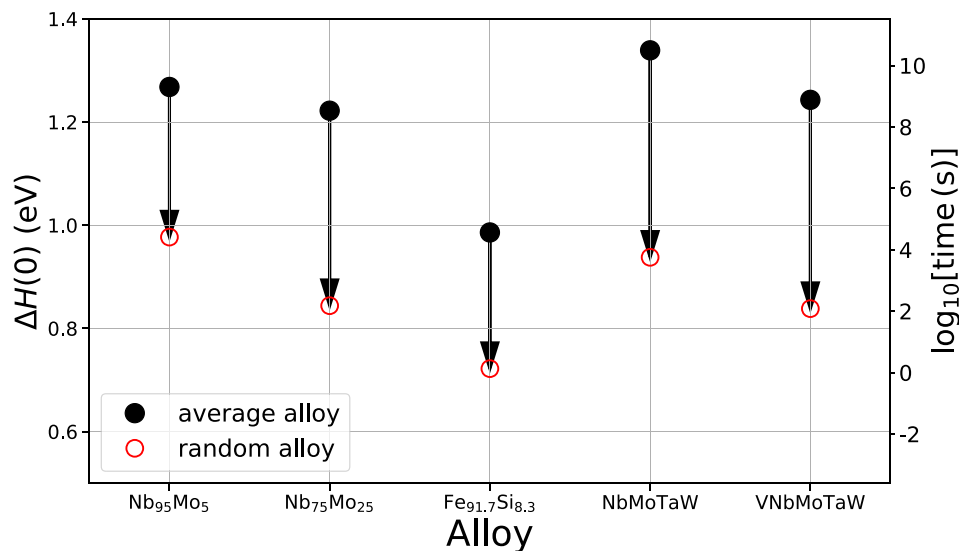
Fig. 13. Double-kink nucleation enthalpy barrier and the time required to move a kink over the length ζ_c at room temperature for various non-dilute complex alloys.

Table 2
The kink formation energy E_k, solute/dislocation interaction energy parameter $\Delta\tilde{E}_p$, characteristic length ζ_c, and the typical energy reduction due to solute fluctuations ($|\Delta\bar{H}^{sol}| + \bar{\sigma}_{\Delta H^{sol}}$) at characteristic length $\zeta_c = Nld_k$, for various non-dilute complex alloys.

Alloy	E_k (eV)	$\Delta\tilde{E}_p$ (meV)	ζ_c/b	$(|\Delta\bar{H}^{sol}| + \bar{\sigma}_{\Delta H^{sol}})/\sigma_{\Delta H^{sol}}$
Nb$_{95}$Mo$_5$	0.634	48.8	198	2.13
Nb$_{75}$Mo$_{25}$	0.611	84.7	61	1.59
Fe$_{91.7}$Si$_{8.3}$	0.493	51.4	108	1.83
NbMoTaW	0.6695	86.2	71	1.66
VNbMoTaW	0.6214	90.6	55	1.59

characteristic length $N = \zeta_c/l_{dk}$, the energy reduction at zero stress due to the solutes can be then estimated from Eqs. (10) and (11) as $\left|\Delta\bar{H}^{sol}(\sigma_{\Delta H^{sol}}, N)\right| + \bar{\sigma}_{\Delta H^{sol}}(\sigma_{\Delta H^{sol}}, N)$, where the standard deviation of the solute energy changes $\bar{\sigma}_{\Delta H^{sol}}$ has been also taken into account and $\sigma_{\Delta H^{sol}} = G(0)\Delta\tilde{E}_p$ is the zero stress standard deviation. For each of the non-dilute complex alloys considered, the energy reduction $\left|\Delta\bar{H}^{sol}\right| + \bar{\sigma}_{\Delta H^{sol}}$ normalized with respect to $\sigma_{\Delta H^{sol}}$ has been computed as shown in Table 2. The time required for the dislocation to kink is the inverse of the nucleation rate $t = 1/R$, where R is given by Eq. (15). We consider room temperature $T = 300\,K$, an attempt frequency $\nu_0 = 10^{12}\,s^{-1}$, and a zero-stress geometrical factor $G(0) = 2.8$.

Fig. (13) shows the double-kink nucleation enthalpy barriers and the time required to move a kink over the length ζ_c at room temperature for various alloys. There is a considerable reduction in the zero stress double-kink nucleation barrier at room temperature for all the non-dilute complex alloys. This leads to a huge reduction in time required for the kink to overcome the nucleation barrier. For instance, the NbMoTaW high-entropy alloy has the largest estimated double-kink nucleation barrier among all these alloys and the solute fluctuations reduce the barrier by ~ 0.4 eV, which decreases the nucleation time from years to less than 2 h (note however that Maresca et al. contend that the strength of this alloy is controlled by edge dislocations [35]). The maximum nucleation time across all alloys is 7 h for the dilute alloy Nb$_{95}$Mo$_5$.

The present analysis thus shows that attaining the low-energy kinked screw structure envisioned by Maresca et al. is facilitated by the reduction of the double-kink nucleation barrier in a complex alloy over the crucial length scale ζ_c. However, at very low temperatures, the time to overcome these barriers remains very large and this may inhibit the transition to the non-dilute low-energy configuration in the Maresca et al. model. This might explain some differences between experiments and the non-dilute theory at T=77K and T=150K at higher solute concentrations where the non-dilute theory is expected to be applicable.

6. Summary

We have developed an analytical theory for the stress-dependent double-kink nucleation barrier in dilute random substitutional BCC alloys as a function of solute concentration and dislocation length, including the range of practical interest (~ $10^3\,b$) where direct atomistic calculations are infeasible. The material parameters in the theory are only (i) the solute/screw dislocation interaction energies, (ii) the transition state configurations of the pure matrix, and (iii) the double-kink enthalpy barrier versus stress for the pure matrix. The theory has been extensively validated on model random Fe-Si alloys with no adjustable parameters. Comparisons to experiment on Fe-Si, W-Re, and W-Ta, have been made and reasonable agreement is obtained at low solute concentrations where double-kink nucleation is expected to control the strength. We further rationalize a transition from softening to hardening with increasing solute concentration as a change in controlling mechanism from double-kink nucleation to a spontaneously kinked structure with strength controlled by kink migration and cross-kink/jog pinning via the model of Maresca et al. This transition involves the same fundamental material parameters in both regimes, and identifies a critical dislocation length scale as determining whether the alloy is in the dilute or non-dilute limit. The present double-kink nucleation model plus the non-dilute model of Maresca et al. together thus provide a single coherent analytic framework within which the initial yield strength in random BCC substitutional alloys can be quantitatively understood when strength is controlled by screw dislocations.

Declaration of Competing Interest

The authors declare that they have no known competing financial interests or personal relationships that could have appeared to influence the work reported in this paper.

Acknowlgedgments

Appendix A. Standard deviation of the potential energy change

In this appendix, we derive the standard deviation of the potential energy change $\sigma_{\Delta U_{tot}}$ when a dislocation segment nucleates over a distance l_{dk} in a random field of solutes, in a dilute binary alloy. The stress-dependent total change in the nucleation barrier due to the nucleation of dislocation is

$$\Delta H^{sol}(\tau) = \sum_{i,j,k} s_{ijk} \Delta U_{ij}(a)\, g(z_k, \tau), \tag{A.1}$$

where the site occupation variable $s_{ijk} = 1$ if a solute is at position (x_i, y_j, z_k) and 0 otherwise. Positions (x_i, y_j, z_k) refer to the atomis sites along one dislocation segment of length l_{dk}. Let $N_s = l_{dk}/b + 1$ denote the number of atomic sites along z direction at each atomic row (x_i, y_j). Also, let label the atoms in each atomic row (x_i, y_j) by $k = 1 \ldots N_s$.

The quantity of interest in the nucleation model is the standard deviation of the total energy change as defined in Eq. (4) which requires $<\Delta H^{sol}>^2$ and $<\Delta H^{sol2}>$. We can write

$$\left\langle \Delta H^{sol} \right\rangle^2 = \sum_{i,j} \sum_k \left\langle s_{ijk} \right\rangle^2 \Delta U_{ij}^2 g(z_k, \tau)^2$$
$$+ \sum_{i,j} \sum_{k,l \neq k} \left\langle s_{ijk} \right\rangle \left\langle s_{ijl} \right\rangle \Delta U_{ij}^2 g(z_k, \tau) g(z_l, \tau)$$
$$+ \sum_{\substack{i,j \\ m,n \neq i,j}} \sum_{k,l} \left\langle s_{ijk} \right\rangle \left\langle s_{mnl} \right\rangle \Delta U_{ij}\, g(z_k, \tau) \Delta U_{mn} g(z_l, \tau) \tag{A.2}$$

$$\left\langle \Delta H^{sol2} \right\rangle = \sum_{i,j} \sum_k \left\langle s_{ijk}^2 \right\rangle \Delta U_{ij}^2 g(z_k, \tau)^2$$
$$+ \sum_{i,j} \sum_{k,l \neq k} \left\langle s_{ijk} s_{ijl} \right\rangle \Delta U_{ij}^2 g(z_k, \tau) g(z_l, \tau)$$
$$+ \sum_{\substack{i,j \\ m,n \neq i,j}} \sum_{k,l} \left\langle s_{ijk} \right\rangle \left\langle s_{mnl} \right\rangle \Delta U_{ij}\, g(z_k, \tau) \Delta U_{mn} g(z_l, \tau) \tag{A.3}$$

The square of the standard deviation of the potential energy change therefore equals

$$\sigma_{\Delta H^{sol}}^2 = \sum_{i,j} \left[\sum_k \left[\left\langle s_{ijk}^2 \right\rangle - \left\langle s_{ijk} \right\rangle^2 \right] \Delta U_{ij}^2 g(z_k, \tau)^2 \right.$$
$$\left. + \sum_{k,l \neq k} \left[\left\langle s_{ijk} s_{ijl} \right\rangle - \left\langle s_{ijk} \right\rangle \left\langle s_{ijl} \right\rangle \right] \Delta U_{ij}^2 g(z_k, \tau) g(z_l, \tau) \right]. \tag{A.4}$$

This result involves the variances and co-variances of the occupation variable s_{ijk}. Note that $\left\langle s_{ijk} \right\rangle = c$. We have

$$\left\langle s_{ijk} s_{ijl} \right\rangle = \sum_k \frac{N_s!}{k!(N_s-k)!} c^k (1-c)^{N_s-k}$$
$$\times \sum_{k_k, k_l} \frac{k!}{k_k! k_l! (k-k_k-k_l)!} \left(\frac{1}{N_s}\right)^{k_k+k_l} \left(1 - \frac{1}{N_s}\right)^{k-k_k-k_l} k_k k_l$$

$$= \sum_k \frac{N_s!}{k!(N_s-k)!} c^k (1-c)^{N_s-k} \left(\frac{1}{N_s}\right)^2 k(k-1)$$
$$= c^2 \left(1 - \frac{1}{N_s}\right), \tag{A.5}$$

with $1 \leq k \leq N_s$ and $0 \leq k_k + k_l \leq k$, and

$$\left\langle s_{ijk}^2 \right\rangle = \sum_k \frac{N_s!}{k!(N_s-k)!} c^k (1-c)^{N_s-k}$$
$$\times \sum_{k_k} \frac{k!}{k_k!(k-k_k)!} \left(\frac{1}{N_s}\right)^{k_k} \left(1 - \frac{1}{N_s}\right)^{k-k_k} k_k^2$$
$$= \sum_k \frac{N_s!}{k!(N_s-k)!} c^k (1-c)^{N_s-k}$$
$$\times \left[\left(\frac{1}{N_s}\right)^2 k^2 + \frac{1}{N_s}\left(1 - \frac{1}{N_s}\right)k \right]$$
$$= \left(\frac{1}{N_s}\right)^2 \left[c^2 N_s^2 + c(1-c)N_s \right] + c\left(1 - \frac{1}{N_s}\right)$$
$$= c + c^2 \left(1 - \frac{1}{N_s}\right), \tag{A.6}$$

with $1 \leq k \leq N_s$ and $0 \leq k_k \leq k$. Inserting Eqs. (A.5) and (A.6) into Eq. (A.4) and neglecting the second order terms in c ($c^2 \ll 1$), we obtain

$$\sigma_{\Delta H^{sol}}^2 = \sum_{i,j} c\, \Delta U_{ij}^2 \sum_k g(z_k, \tau)^2 \tag{A.7}$$

Finally, by defining the $z = 0$ to be located right at the double-kink nucleus, the above equation can be rewritten as

$$\sigma_{\Delta U_{sol}}^2 = \sum_{i,j} c\, \Delta U_{ij}^2 \sum_{k=-N_s}^{N_s} g(kb, \tau)^2. \tag{A.8}$$

Here, $N_s = l_{dk}/(2b)$.

Appendix B. Double-kink nucleation rate

The total double-kink nucleation rate is the sum of the rates of all N nucleation sites which can be described as

$$R = \nu_0 N \exp\left(-\frac{\Delta H^0(\tau)}{kT}\right) \int_{\Delta \bar{H}^{sol}(c,N,\tau)}^{\infty} d\Delta H P[\Delta H] \exp\left(-\frac{\Delta H}{kT}\right), \tag{B.1}$$

where $P[\Delta H]$ is the probability of finding the double-kink nucleation segment with solute energy change ΔH given by Eq. (8). After some manupulations the above equation can be rewritten as Eq. (9). It is of interest to find the temperature T_0 below which the weakest link dominates and thus the rate can be expressed by (15). To this end, we use the following approximated form for erfc(x) [36]

$$\text{erfc}(x) \approx \frac{(1 - e^{-1.98x})e^{-x^2}}{1.135\sqrt{\pi}x} \tag{B.2}$$

Substitiong the above relation into Eq. (9) and equating the resultant equation with Eq. (15), gives the following solution for T_0 which is the temperature at which the two representations of double-kink nucleation rate become equal

$$\frac{kT_0}{\sigma_{\Delta H^{sol}}(c,\tau)}$$
$$= \left(0.35 N e^{-\frac{c_N^2}{2}} + 0.7 W\left[-0.5 N \exp\left(-0.5 N e^{-\frac{c_N^2}{2}} - \frac{c_N^2}{2} \right) \right] - c_N \right)^{-1} \tag{B.3}$$

where $W[\,\cdot\,]$ stands for the Lambert W-function and $c_N = b_N - \gamma a_N$. This temperature is approximately $kT_0 = 0.255\, \sigma_{\Delta H^{sol}}$ over a

wide range of N. However, since $\sigma_{\Delta H^{\mathrm{sol}}}(c, \tau)$ depends on the applied stress τ which is not known a-priori, the exact computation of the cross-over temperature is not possible. It can be shown that, to a high approximation, T_0 can be obtained by solving the following equation

$$\Delta H_{\mathrm{exp}}^0(\tau) = 0.255 \, \sigma_{\Delta H^{\mathrm{sol}}}(c, \tau) \log \left[250 \frac{\dot{\epsilon}_0}{\dot{\epsilon}} \right].$$

The above equation gives the yield stress at temperature T_0 from which $\sigma_{\Delta H^{\mathrm{sol}}}$ and thus T_0 can be computed.

Appendix C. Simulation details of NEB calculations

To compute the minimum energy path (MEP) connecting the initial and final states, nudged elastic band (NEB) computations [37–40] are performed as implemented in LAMMPS [41] using the interatomic potential developed by [2]. MEP calculations were started as follows. Using the Fe lattice parameter, a rectangular simulation cell oriented with $[1\bar{1}2]$ along the glide direction X, [110] along the glide plane normal direction Y, and $[\bar{1}11]$ along the dislocation line direction Z, was constructed. Periodic boundary conditions are imposed along X and Z directions, and Y having imposed tractions. The simulation cell has dimensions $L_1 \sim 110A$ and $L_2 \sim 100A$ and L_3 depends on the dislocation length. A screw dislocation of Burgers vector $a/2[111]$ with line direction along Z is then introduced into the center of the cell by imposing a linear displacement $u_z = -bx/l_x$ for $0 < x < l_x$ on all atoms in the upper half of the simulation cell. This generates the initial atomic configuration. The final state has the same structure as the initial state but shifted by a relative to the initial state. Atomic positions are then relaxed by using a combination of the FIRE algorithm [42] and relaxation of the cell dimensions. Convergence is achieved when the norm of the force vector fell below 10^{-6} eV/A and stresses σ_{XX}, σ_{XY}, and σ_{YY} fell below 0.1 MPa. The above initial and final states are used as templates to carry out the MEP calculations. In order to model the Fe-Si dilute alloys, the Fe atoms in initial state configurations were replaced randomly by Si solutes at the desired alloy concentration. Accordingly, the same Fe solutes were replaced by Si atoms in the final state. The energy of the initial and final alloy configurations were then minimized using CG and FIRE with the same tolerences on forces and stresses as specified above. NEB simulations are performed using 60 replicas. An initial path of intermediate configurations (replicas) is constructed by linearly interpolating the atomic positions between the relaxed initial and final states. The NEB inter-replica spring constant is set to 10^{-2} eV/Å^2 and convergence is assumed when the maximum of the force acting on all of the atoms across all replicas is less than 1×10^{-3} eV/Å.

References

[1] D.R. Trinkle, The chemistry of deformation: how solutes soften pure metals, Science 310 (5754) (2005) 1665–1667.
[2] S. Shinzato, M. Wakeda, S. Ogata, An atomistically informed kinetic Monte Carlo model for predicting solid solution strengthening of body-centered cubic alloys, Int. J. Plast. 122 (2019) 319–337.
[3] Y. Zhao, J. Marian, Direct prediction of the solute softening-to-hardening transition in w–re alloys using stochastic simulations of screw dislocation motion, Modell. Simul. Mater. Sci. Eng. 26 (4) (2018) 045002.
[4] J. Weertman, Dislocation model of low-temperature creep, J. Appl. Phys. 29 (12) (1958) 1685–1689.
[5] E. Pink, Low-temperature softening in body-centered cubic alloys, Prog. Mater. Sci. 24 (1) (1979) 1–50.
[6] H. Suzuki, Solid solution hardening in body-centred cubic alloys, Dislocations Solids 4 (1980) 191–217.
[7] J.R. Stephens, Dislocation structures in single-crystal tungsten and tungsten alloys, Metall. Mater. Trans. B 1 (5) (1970) 1293–1301.
[8] Y.-J. Hu, M.R. Fellinger, B.G. Butler, Y. Wang, K.A. Darling, L.J. Kecskes, D.R. Trinkle, Z.-K. Liu, Solute-induced solid-solution softening and hardening in BCC tungsten, Acta Mater. 141 (2017) 304–316.
[9] A. Argon, Strengthening Mechanisms in Crystal Plasticity, 4, Oxford University Press on Demand, 2008.
[10] L. Romaner, C. Ambrosch-Draxl, R. Pippan, Effect of rhenium on the dislocation core structure in tungsten, Phys. Rev. Lett. 104 (19) (2010) 195503.
[11] L. Romaner, Unpublished research.
[12] M. Hossain, J. Marian, Stress-dependent solute energetics in w–re alloys from first-principles calculations, Acta Mater. 80 (2014) 107–117.
[13] T. Tsuru, T. Suzudo, First-principles calculations of interaction between solutes and dislocations in tungsten, Nucl. Mater. Energy 16 (2018) 221–225.
[14] S. Rao, B. Akdim, E. Antillon, C. Woodward, T. Parthasarathy, O. Senkov, Modeling solution hardening in BCC refractory complex concentrated alloys: NbTiZr, Nb1.5TiZr0.5 and Nb0.5TiZr1.5, Acta Mater. 168 (2019) 222–236.
[15] H. Li, S. Wurster, C. Motz, L. Romaner, C. Ambrosch-Draxl, R. Pippan, Dislocation-core symmetry and slip planes in tungsten alloys: ab initio calculations and microcantilever bending experiments, Acta Mater. 60 (2) (2012) 748–758.
[16] F. Maresca, W.A. Curtin, Theory of screw dislocation strengthening in random BCC alloys from dilute to æhigh-entropyg alloys, Acta Mater. 182 (2020) 144–162.
[17] Y.-J. Hu, Z.-K. Liu, Personal Communication, 2019.
[18] L. Dezerald, L. Proville, L. Ventelon, F. Willaime, D. Rodney, First-principles prediction of kink-pair activation enthalpy on screw dislocations in BCC transition metals: v, nb, ta, mo, w, and fe, Phys. Rev. B 91 (9) (2015) 094105.
[19] L. Proville, D. Rodney, M.-C. Marinica, Quantum effect on thermally activated glide of dislocations, Nat. Mater. 11 (10) (2012) 845–849.
[20] F. Maresca, D. Dragoni, G. Csányi, N. Marzari, W.A. Curtin, Screw dislocation structure and mobility in body centered cubic fe predicted by a gaussian approximation potential, Npj Comput. Mater. 4 (1) (2018) 1–7.
[21] U.F. Kocks, A. AS, A. MF, Thermodynamics and Kinetics of Slip, 1975.
[22] L. Ventelon, F. Willaime, E. Clouet, D. Rodney, Ab initio investigation of the peierls potential of screw dislocations in bcc fe and w, Acta Mater. 61 (11) (2013) 3973–3985.
[23] A. Ghafarollahi, F. Maresca, W. Curtin, Solute/screw dislocation interaction energy parameter for strengthening in BCC dilute to high entropy alloys, Modell. Simul. Mater. Sci. Eng. 27 (8) (2019) 085011.
[24] K. Kitajima, Y. Aono, H. Abe, E. Kuramoto, Solid Solution Hardening and Softening in Iron Alloy Single Crystals between 4.2 K and 300 K, in: Strength of Metals and Alloys, Elsevier, 1979, pp. 965–970.
[25] S. Takeuchi, Solid-solution strengthening in single crystals of iron alloys, J. Phys. Soc. Jpn. 27 (4) (1969) 929–940.
[26] H. Koizumi, H. Kirchner, T. Suzuki, Kink pair nucleation and critical shear stress, Acta Metall. Mater. 41 (12) (1993) 3483–3493.
[27] D. Brunner, J. Diehl, The effect of atomic lattice defects on the softening phenomena of high-purity α-iron, Physica Status Solidi (a) 160 (2) (1997) 355–372.
[28] D. Caillard, A TEM in situ study of alloying effects in iron. Solid solution softening caused by low concentrations of Ni, Si and Cr, Acta Mater 61 (8) (2013) 2793–2807.
[29] S. Takeuchi, H. Yoshida, T. Taoka, Solid-solution strengthening in iron alloys, Trans.e Jpn Inst. Metals Suppl. 9 (1968) 715–719.
[30] Y. Chen, D. Atteridge, W.W. Gerberich, Plastic flow of fe-binary alloysi. A description at low temperatures, Acta Metall. 29 (6) (1981) 1171–1185.
[31] A. Stukowski, D. Cereceda, T.D. Swinburne, J. Marian, Thermally-activated non-schmid glide of screw dislocations in w using atomistically-informed kinetic monte carlo simulations, Int. J. Plast. 65 (2015) 108–130.
[32] W.J. Szlachta, A.P. Bartók, G. Csányi, Accuracy and transferability of Gaussian approximation potential models for tungsten, Phys. Rev. B 90 (10) (2014) 104108.
[33] P.L. Raffo, Yielding and fracture in tungsten and tungsten-rhenium alloys, J. Less Common Metals 17 (2) (1969) 133–149.
[34] J.R. Stephens, W.R. Witzke, Alloy softening in group via metals alloyed with rhenium, J. Less Common Metals 23 (4) (1971) 325–342.
[35] F. Maresca, W.A. Curtin, Mechanistic origin of high strength in refractory BCC high entropy alloys up to 1900k, Acta Mater. 182 (2020) 235–249.
[36] G.K. Karagiannidis, A.S. Lioumpas, An improved approximation for the Gaussian q-function, IEEE Commun. Lett. 11 (8) (2007) 644–646.
[37] G. Henkelman, H. Jónsson, Improved tangent estimate in the nudged elastic band method for finding minimum energy paths and saddle points, J. Chem. Phys. 113 (22) (2000) 9978–9985.
[38] G. Henkelman, B.P. Uberuaga, H. Jónsson, A climbing image nudged elastic band method for finding saddle points and minimum energy paths, J. Chem. Phys. 113 (22) (2000) 9901–9904.
[39] A. Nakano, A space–time-ensemble parallel nudged elastic band algorithm for molecular kinetics simulation, Comput. Phys. Commun. 178 (4) (2008) 280–289.
[40] E. Maras, O. Trushin, A. Stukowski, T. Ala-Nissila, H. Jonsson, Global transition path search for dislocation formation in Ge on Si (001), Comput. Phys. Commun. 205 (2016) 13–21.
[41] S. Plimpton, Fast parallel algorithms for short-range molecular dynamics, Technical Report, Sandia National Labs., Albuquerque, NM (United States), 1993.
[42] E. Bitzek, P. Koskinen, F. Gähler, M. Moseler, P. Gumbsch, Structural relaxation made simple, Phys. Rev. Lett. 97 (17) (2006) 170201.